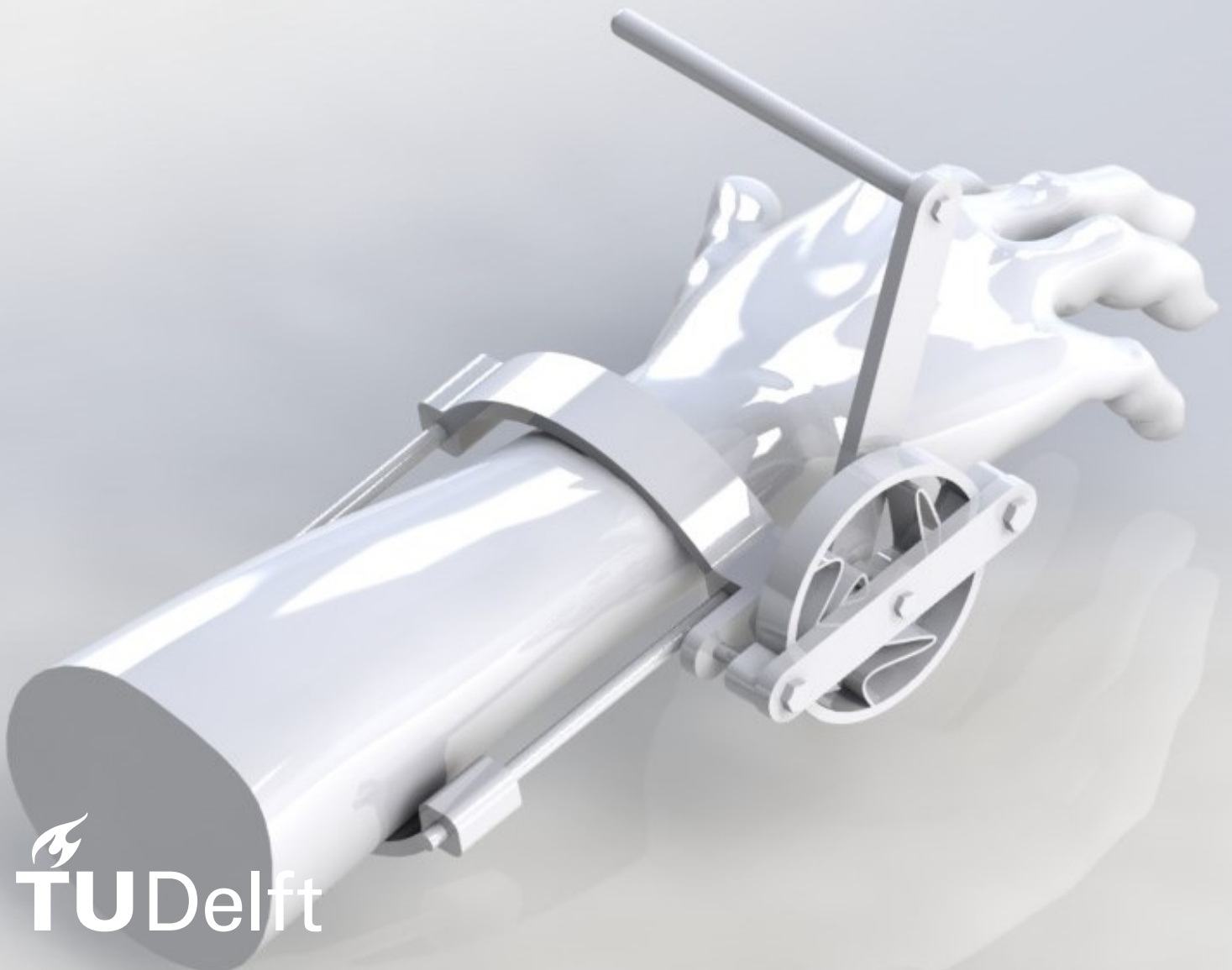


Constant Torque Mechanism for Gravity Balancing in Wrist Support Application

Dhanush Chitluri

Delft University of Technology



Department of Precision and Microsystems Engineering

Constant Torque Mechanism for Gravity Balancing in
Wrist Support Application

Dhanush Chitluri

Report no : 2023.076
Coach : Ir. A. Amoozandeh Nobaveh,
Professor : Prof. Dr. ir. J. L Herder
Specialisation : MSD
Type of report : Thesis report
Date : 16-08-2023

Constant Torque Mechanism for Gravity Balancing in Wrist Support Application

by

Dhanush Chitluri

5481031

Thesis Committee : Prof.Dr.Ir.J.L Herder, TUDelft, supervisor

Ir.A.Amoozandeh Nobaveh, TUDelft, daily supervisor

Dr.Ir.G.Radaelli, TUDelft, daily supervisor

Dr.Ir.R.A.J. (Ron) van Ostayen, Thesis committee member

ProjectDuration : September2022 – August2023

Preface

To conclude the chapter of my academic voyage as a student, this work has been undertaken as a part of my master's thesis at the Delft University of Technology, symbolizing the culmination of my educational journey.

With the dream of pursuing higher learning and personal growth, this thesis work marks a journey that has enriched my understanding of educational theories and practices and ignited a sincere passion for contributing to the field. I am deeply grateful for the support, guidance, and inspiration I have received throughout this endeavour, especially from my esteemed professors. Undertaking this thesis would not have been possible without the unwavering encouragement and expertise of my dedicated professors at TU Delft. First, I would like to thank my supervisors, Ir. A. Amoozandeh Nobaveh, Dr. Ir. G. Radaelli, and Prof. Dr. ir. J. L. Herder for their valuable guidance throughout the project and insightful feedback during the weekly meetings and brainstorming team meetings, which have been instrumental in shaping my research trajectory and enhancing the quality of this work.

I would also like to express my gratitude to Sjaak Kok from YUMEN Bionics, my peers and fellow students, whose diverse perspectives and stimulating discussions have contributed immeasurably to my intellectual growth. With this thesis, I aspire to make a meaningful contribution to the field of exoskeletons, guided by the conviction that it is indeed the most powerful instrument for positive change and adds a reference to future works.

With deep respect and heartfelt gratitude,
Dhanush Chitluri
Delft, August 2023

Summary

A group of muscular disorders caused by a genetic mutation in individuals significantly impacts limb muscle strength and, thus, their daily activities. Duchenne muscular dystrophy (DMD) is a disease that predominantly affects male children due to the lack of protein in the muscle fibres. The onset of this disorder can severely impair upper and lower limb functionality, negatively impacting joint stiffness and range of motion of the limbs. To alleviate such challenges, assistive technologies like orthoses and exoskeletons support and augment limb movements. The arm, a crucial component responsible for many daily activities, characterizes the upper extremity of the human body. Within this arm structure lies the wrist, located between the forearm and hand and comprising muscles and intricate bones that govern forearm, wrist, and finger movements. This sophisticated joint system offers remarkable mobility, underlining the importance of its proper functioning. Within this realm, wrist support devices are pivotal in aiding flexion and extension, especially for individuals with limited mobility due to conditions such as Duchenne muscular dystrophy (DMD).

The research begins with a comprehensive exploration of the arm's joint structure, degrees of freedom, wrist kinematics and kinetics. With a comprehensive understanding, the study is centred on achieving a constant torque output throughout the desired wrist motion range during flexion/extension.

A novel approach is introduced to provide wrist support by counteracting gravitational forces during wrist flexion and extension. The research focuses on creating a compliant mechanism for wrist support, aiming to mitigate muscle-weakening effects and enhance wrist stability. The curvature of the flexure in the mechanism notably influences flexure deflection, thereby impacting torque deflection behaviour. The methodology involves an initial random search to capture diverse design space samples, then refinement of the generated designs. This endeavour utilizes an optimization-based design methodology, gauging the error between the intended and actual torque-deflection behaviours. The ultimate aim is to identify designs approximating the best possible solutions.

Experimental validation is a cornerstone of the research. A prototype is developed for practical testing of the mechanism. The prototype is fabricated through 3D printing, employing PLA material and the FDM method to create a scaled-up model. This prototype's performance is meticulously evaluated, showcasing its potential to meet torque requirements. An elaborate testing setup ensures stability and accurate torque measurement. This setup closely emulates real-world conditions, minimizing potential discrepancies that could compromise data accuracy. Applying designated boundary conditions, data is collected and analyzed by comparing it with results from optimization techniques.

However, future research on wrist support using the compliant mechanism could reduce the simplifications and assumptions followed in this research.

Contents

Preface	i
Summary	ii
1 Introduction	1
1.1 Duchenne Muscular Dystrophy	2
1.2 Functioning Level	3
1.3 Treatments	3
2 Literature Review	6
3 Research Paper	21
4 Conclusion	34
4.1 Contribution	34
4.2 Future work	34
A Experimental setup	36
A.1 Test Protocol	36
A.2 Fixing the compliant mechanism	37
A.3 Input torque	38
A.4 Final setup	39
B Analysis Results	40
B.1 Stress analysis	40
C Development and Manufacturing:	42
C.1 Prototype development	42
C.2 Prototype manufacturing	43
D Positive and Negative stiffness mechanism	44
D.1 Introduction	44
D.2 Model	44

1

Introduction

1.1. Duchenne Muscular Dystrophy

Muscular dystrophies are inherited genetic disorders caused by mutations in a group of muscles, resulting in a greater impact on people's lives (both males and females of all ages). This condition weakens and progressively wastes the muscles, making muscle control and movement difficult. Various dystrophies are caused by X-linked disorders, including congenital, myotonic, Limb and girdle, Facioscapulohumeral, Emery–Dreifuss, Distal, Oculopharyngeal, Duchenne, Becker, and Collagen Type VI-Related disorders. Although various types of diseases exist, they are further subdivided into several groups based on the congenital form and disease propagation. Some of them are less sensitive and progress slowly over time, not having a severe effect on muscle movement or control, while others have a rapid progression of the disease, causing muscle wastage and physical disablement, reducing life expectancy, and sometimes leading to heart failure [14] [7].

Among all the diseases, DMD (Duchenne muscular dystrophy) is one of the most common recessive inherited diseases caused by a mutation leading to the lack of protein in the skeletal muscle fibres (dystrophin) set down on the X-chromosome [13]. Thousands of different mutations are found in DMD patients, including more extensive genomic rearrangements between an X chromosome, deletions, and some small mutations. Since these are X-linked disorders, most mutations predominantly affect boys, occurring in approximately 1 in 5000 to 1 in 6000 male births [3][9]. Symptoms that appear in individuals with growth in age are Frequent falls, Difficulty rising from a lying or sitting position, Trouble running and jumping, Waddling gait, Walking on the toes, Large calf muscles, Muscle pain and stiffness, Learning disabilities, Delayed growth [8].

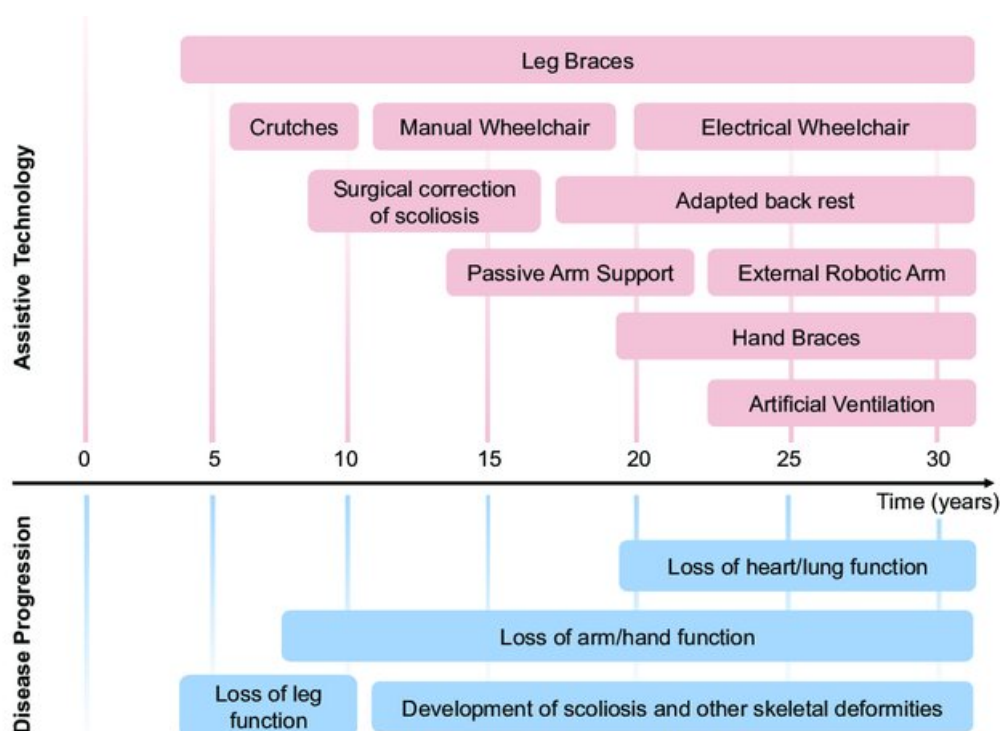


Figure 1.1: Assistive technology is employed based on the individual's level of functionality and specific needs [10].

The progression of this disease starts in childhood, typically manifesting by the age of 2-3, and by the age of 5, affected individuals start experiencing difficulty in walking. With increasing age, there is a significant drop in muscle control and limb strength, resulting in imbalances and an increased risk of developing contractures and deformities, which can lead to cardiac arrests and heart failures in some cases. Besides skeletal muscle wastage, these patients also experience respiratory issues

that progressively worsen from the early 20s. The progression of the disease is depicted in Figure 1.1. The average life span of patients with DMD is expected to be as low as 25 years; however, advances in treatment methods have increased the average life expectancy of these patients to 30 to 40 years. Nonetheless, the most common cause of death is heart failure, such as cardiac arrests or lung failures, including respiratory complications, pneumonia, aspiration, or airway obstructions.

1.2. Functioning Level

From the previous discussions, it has been observed that the disease progresses by affecting the functionality of the muscles, causing pain and an increase in muscle stiffness, thereby reducing an individual's ability to perform daily activities [5]. Clinical studies and research using specific scales, such as the Brookes scale and Vignos scale [12], estimate the functionality degradation in both the upper and lower limbs. However, these scales are not considered ideal. Nonetheless, they allow the health-care sector to assess and monitor the functionality of the limbs and track the disease's progression in individuals.

Scale in levels	Effect in functioning
Level 1	Exhibits normal upper body function and is capable of raising their arms above their head without any difficulty or limitations.
Level 2	Experiences mild to moderate difficulty in raising their arms completely above their head.
Level 3	Unable to raise their arms above shoulder level and limited arm movement.
Level 4	Has limited arm movement
Level 5	Lacks functional use of their arms, but they retain the ability to use their hands effectively
Level 6	No proper functioning of both hands and arms

Table 1.1: Brookes upper extremity rating scale based on the functionality

The interest of this paper is on the wrist, so, as mentioned earlier, the Brookes scale assesses the functionality of the upper limbs and the progression of the disease [1]. The following Table 1.2 explains the categorization of upper limb functioning levels:

1.3. Treatments

There is no specific cure for DMD (Duchenne muscular dystrophy). The treatment aims to reduce the propagation speed of the disease, i.e., control symptoms, improve the quality of life, and assist patients in performing daily activities smoothly. There are limited treatments available for DMD patients, including interventions such as low-impact exercises like swimming and regular recreational exercises to prevent muscle wastage, physical therapy to regain muscle strength and avoid contractures [9], and aids and assistive devices such as wheelchairs, leg braces, and arm braces Figure 1.1. The medical terms for the earlier treatments can be categorized as drug-based, physical, respiratory, occupational, speech, gene-based, and surgery [2], [4].

Also, medications, such as corticosteroids (such as glucocorticoids, prednisone/prednisolone, and deflazacort), anticonvulsants, and immunosuppressants, are commonly used for DMD patients. However, these medications may have some side effects, as they tend to slow down the progression of the disease and increase life span.

It's crucial to emphasize that while these treatments hold the potential to enhance the quality of life and mitigate the progression of DMD, they do not constitute a definitive cure for the condition. Ongoing research and strides in the realm of medical science persist in pursuing more efficacious treatments and potential remedies for this intricate disorder. As previously discussed, applying exoskeletons and orthoses for rehabilitation is prominent alongside these treatment innovations. The development of exoskeletons represents a significant endeavour in the field. However, the challenge of effectively balancing the weight on the hand has limited the availability of viable wrist support solutions. This challenge arises from the dynamic nature of wrist torque changes due to hand position variations. In the ensuing sections of this paper, attention is directed toward developing a specific device within this context. This device, elucidated in the subsequent chapters, manifests as a significant step in the quest to provide enhanced support and functional assistance for individuals grappling with DMD.

An extensive study has been conducted to gain a profound comprehension of wrist kinematics and kinetics. Utilizing insights from these investigations, a simplified representation of wrist kinetics has been developed, focusing on a specific degree of freedom of the hand whose motion is against gravity, namely, flexion and extension. Alongside the study on the wrist, a comprehensive and thorough literature review has been undertaken to investigate a wide array of variable stiffness mechanisms and the mechanisms that facilitate constant force and torque from various applications.

The imperative need for a gravity balancing mechanism intended to counteract the force of gravity during hand movements emerges from this analytical groundwork. After the development of the model using parametric optimization, seamless integration of the mechanism with the intended device has been achieved. This amalgamation serves the crucial purpose of supporting the hand against gravity, thus enabling smoother and more controlled hand motion.

Bibliography

- [1] Michael H Brooke et al. "Clinical trial in Duchenne dystrophy. I. The design of the protocol". In: *Muscle & Nerve: Official Journal of the American Association of Electrodiagnostic Medicine* 4.3 (1981), pp. 186–197.
- [2] Cleveland Clinic. *Professional, C.C. medical, Duchenne muscular dystrophy (DMD): Symptoms amp.* <https://my.clevelandclinic.org/health/diseases/23538-duchenne-muscular-dystrophy-dmd>.
- [3] Dongsheng Duan et al. "Duchenne muscular dystrophy". In: *Nature Reviews Disease Primers* 7.1 (2021), p. 13.
- [4] Eunice Kennedy Shriver. *National Institute of Child Health and Human Development.* <https://www.nichd.nih.gov/health/topics/musculardys/conditioninfo/treatment>.
- [5] WV James and JF Orr. "Upper limb weakness in children with Duchenne muscular dystrophy—a neglected problem". In: *Prosthetics and orthotics international* 8.2 (1984), pp. 111–113.
- [6] Brian D Jensen and Larry L Howell. "Bistable configurations of compliant mechanisms modeled using four links and translational joints". In: *J. Mech. Des.* 126.4 (2004), pp. 657–666.
- [7] Agnieszka Łoboda and Józef Dulak. "Muscle and cardiac therapeutic strategies for Duchenne muscular dystrophy: past, present, and future". In: *Pharmacological Reports* 72 (2020), pp. 1227–1263.
- [8] Mayo Foundation for Medical Education and Research. *Muscular dystrophy by Mayo Clinic.* <https://www.mayoclinic.org/diseases-conditions/muscular-dystrophy/symptoms-causes/syc-20375388>. 1998.
- [9] NHS choices. *NHS choices.* <https://www.nhs.uk/conditions/muscular-dystrophy/treatment/>.
- [10] Joan Lobo Prat. *Control interfaces to actively support the arm function of men with Duchenne muscular dystrophy.* University of Twente, 2016.
- [11] Saquib Rouf et al. "3D printed parts and mechanical properties: Influencing parameters, sustainability aspects, global market scenario, challenges and applications". In: *Advanced Industrial and Engineering Polymer Research* 5.3 (2022), pp. 143–158.
- [12] Dilan Savaş and Tülay Tarsuslu Şimşek. "Functional level and its relationship to upper extremity function, pain, and muscle stiffness in children with Duchenne muscular dystrophy". In: *Irish Journal of Medical Science (1971-)* (2022), pp. 1–7.
- [13] Hideo Sugita and Shin'ichi TAKEDA. "Progress in muscular dystrophy research with special emphasis on gene therapy". In: *Proceedings of the Japan Academy, Series B* 86.7 (2010), pp. 748–756.
- [14] Eppie M Yiu and Andrew J Kornberg. "Duchenne muscular dystrophy". In: *Journal of paediatrics and child health* 51.8 (2015), pp. 759–764.

2

Literature Review

Literature Review on Variable Stiffness, Constant Force and Constant Torque Mechanisms in Various Applications

Dhanush Chitluri (5481031)
Department of Precision and Microsystems Engineering
Delft University of Technology
Delft, The Netherlands
D.chitluri@student.tudelft.nl

Abstract—To provide support or assistance with rehabilitation for people affected by neuromuscular disorders. There are many exoskeletons or orthoses for arms and legs but a limited number of devices for wrist support. This is because of the complexity of design for the number of degrees of freedom (DOF) that are to be supported in a limited space without any constraints. In this review, different passive and semi-passive variable stiffness mechanisms in different applications were studied and sorted by making an overview, evaluation, and comparison based on the parameters such as weight, size, stiffness range, and adaptability in designing. The review showed that there are only a few conceptual solutions that can be used to develop wrist support using the variable stiffness mechanisms.

Index Terms—variable stiffness, controllable stiffness, constant force, constant torque, preload/pre-tension, energy, wrist, arm, orthoses, and exoskeleton.

I. INTRODUCTION

A muscular dystrophy is a group of genetically heterogeneous muscle diseases that seriously impact people's lives by continuously wasting and weakening the skeletal muscle, smooth muscles, or other tissues and sometimes cause cardiac arrests or strokes[54]. Duchenne Muscular Dystrophy (DMD) is one of the common diseases that is caused among children with an incidence of 1 in 3500 to 1 in 5000 male births [14, 12, 31]. The initial sign of disease starts before age 5 by losing the ability to walk, followed by this, the control groups and grip strengths [37] slowly have a significant drop in the boys aged between 4-21, which results in the imbalance between the muscles has a risk of leading to the development of contractures and deformities [58] and decreases the patient's ability to carry out the manual activities. Because of this progressive muscle debility, they rely on orthoses or exoskeletons for smooth running of daily activities. But the device requirement depends on the type of disease and the progression of the weakness, some patients are in the need of compensation for the weight of the arm and hand while others need it for the increased stiffness in muscles and joints (due to contractures). The weight compensation is used to support the weakened muscles and the remaining muscle strength is used to move the hand whereas to improve the motion in case of stiffened muscles, the negative stiffness springs are used [18]. In the devices that are used for rehabilitation, some form

of a mechanism is used for balancing the weight or stiffness [41, 30] and thus, the review is focused on the concepts that are providing the support by balancing using variable stiffness mechanisms.

Many exoskeletons and their literature are available: Aaron et al. [11], Seyfarth [52] and Daniel et al. [15] have done work on the development of various passive and active wearable devices for legs. Similarly, Heide et al. [57] and Gull et al. [19] have presented an overview of dynamic upper limb supports, also from their work it was found that very few have been commercially available. However, ample use of these devices in daily activities might lead to the progression of diseases, so it is not suggested to use these devices on regular basis. Most of these devices use active systems for upper limbs such as arms[46], back[48], and hand[50], and an extensive study has been made on the active hand exoskeletons by du Plessis et al. [47], but from the literature, it is realized that there are very limited resources on passive wrist exoskeletons. Nevertheless, there are some of passive wrist exoskeletons that are commercially available: "Dynamplint", "Prim" and "Ambroise" Dynamic Wrist Orthosis compensates for the weight of the hand with weakened muscles. However, there are certain limitations with these devices, like they can only work in a particular orientation of the forearm and perform only specific functions. Thus, the wrist is a complex joint having 1) different orientations because of the shoulder, elbow, and forearm movements, and thus, the load vector on the hand changes, and it becomes difficult to balance the weight of the hand. 2) limited design space (size of the device is restricted), and 3) a large range of motion (chances of misalignment in joints). So, designing the wrist support not only need weight compensation but perhaps needs constant load support in every orientation of the forearm considering the design space and for this reason, a variable stiffness mechanism can be used to develop the wrist support.

The aim of this review is to find a variable stiffness mechanism concept that can be used to support the wrist. The variable stiffness mechanism can be completely passive [34, 43, 44, 36] or can be semi-active [61, 2] or completely active [5,

4]. In active balancing mechanisms, the force required to balance the system is provided by the actuators whereas there is no need for any external energy to control the stiffness in passive mechanisms, as the potential energy is kept constant by changing the form from one to another: kinetic energy to strain energy. But unlike the active system, in the case of semi-active mechanisms, the external energy is used to change the stiffness of the mechanism (inter-disciplinary such as the hydraulic or magnetic force on a mechanical design) and thus, changes the output force. However, there are limited resources on the passive variable stiffness mechanisms and so, this review mainly focuses on the passive variable stiffness mechanisms and the semi-active variable stiffness mechanisms. These mechanisms are further evaluated and compared based on their applicability on the wrist for weight and stiffness compensation.

subsection II-A describes the categorization made based on the working principles and concepts of variable stiffness structures. In section II the concepts found in the literature are explained and classified through the categorization as established in subsection II-A. In subsection II-B, a flowchart has been used to show the subcategories of the categorization for the concepts presented in section II, and also, based on certain parameters, a comparison table has been implemented for the concepts mentioned in section II. The concepts that have been proposed in section II are evaluated based on the performance indicators and have been compared. In addition, the comparison of this review is later discussed in section III based on its advantages, limitations, and gaps in the literature.

II. METHODS

In this section, a categorization of the concepts found in the literature is discussed.

A. Classification

During the literature search on the variable stiffness mechanisms and from [32, 22, 60], the following categorization has been made, as it is found that the stiffness control is done based on three factors: Figure 2: 1) Material Properties, 2) Shape and 3) Boundary conditions. In Figure 1, based on these classifications and the number of concepts found in the literature, a pie chart has been made. The number of concepts found on variable stiffness mechanisms is mentioned in this chart, and thus, it has passive, semi-active and active mechanisms.

The factors mentioned in Figure 1 lead to the change of the stiffness in each of these concepts and these mechanisms that have been used in different applications. Further, in this section, the working principle of these mentioned concepts has been described along with an application and is sub-categorized to one of the categories in the Figure 2.

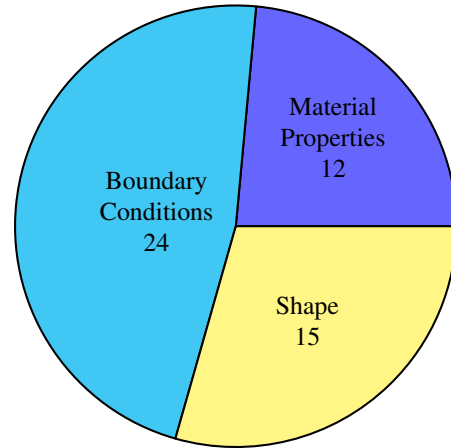


Fig. 1: Pie chart showing the number of concepts found per classification

1) Tri-stable structure:

A tri-stable structure has three equilibrium states (stable configurations): plane, concave and convex states that have been designed and proposed by Fuhong et al. [7]. From the investigation of Hyer et al. [24],[25] and [23], a bi-stable structure has two natural equilibrium points without the need for any external power, and the energy required is quite less for large deflections[65]. The tri-stable mechanism not only snaps in and out due to bending but can also be twisted [51]. In the tri-stable model, four rectangular bi-stable laminates are arranged in an unsymmetrical configuration as shown in Figure 3. This starts as a base model for building multi-stable structures with complex layouts that consist of tri-stable structures as unit cells[38]. The first equilibrium state is the initial configuration i.e, the plane configuration, whereas the other two equilibrium states are the concave and convex configurations which are achieved by lowering the bending stiffness of the initial configuration as the elasticity of the structure depends on the geometry and certain boundary conditions. The snap-in or snap-out motion of the tri-stable structure from the plane motion exhibits large strain when a transverse or longitudinal load is applied and thus, it is an energy-efficient shape-morphing structure.

2) Bi-stable flap design:

A bi-stable flap concept is used in airfoil sections. Daynes et al [8] developed a design by stacking six bistable prestressed buckled laminates with $[0/90/90/0]_T$ in an asymmetric order. These laminates are manufactured by inducing a pre-strain of 1.1%, which is used for flapping the laminates from first stable configuration i.e, the initial configuration: 0^0 to the second stable configuration i.e, deformed configuration: 10^0 as shown in Figure 4. Besides the camber morphing, the advancement of the airfoils has been done by Diaconu et al. in [9] & [10] introduces two concepts for trailing edge and chord length morphing. By changing the orientation of

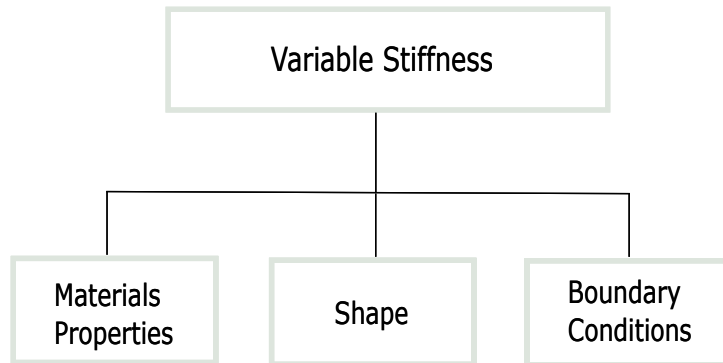


Fig. 2: Categorization based on the literature found on variable stiffness mechanisms

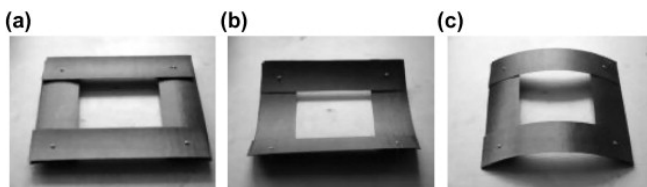


Fig. 3: Tri-stable structure with all the 3 configurations. a) Plane configuration b) Concave configuration c) Convex configuration

the bi-stable plate (one horizontally and the second vertically with 90^0 rotation) as shown in Figure 5 for camber and Figure 6 for chord length (geometry) morphing takes place. The following factors were considered while developing these structures such as the load-carrying capacity to sustain the aerodynamics, temperature, moisture in the environment, and the overall torsional stiffness. Arrieta et al.[1] explained the dynamic control of the morphing of bistable structures, as the modal frequencies for the asymmetrically arranged laminates might affect the dynamics and leads to chaos. By selecting the distinct modal frequencies, chaotic oscillations will be reduced during shape morphing.

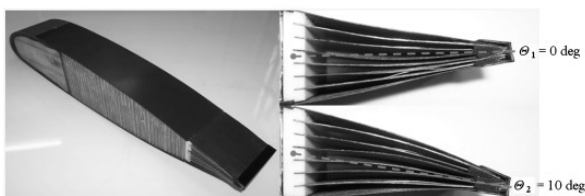


Fig. 4: Bi-stable flap conceptual design

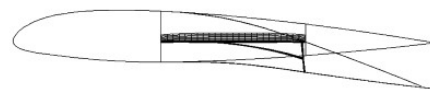


Fig. 5: Lateral view of camber morphing

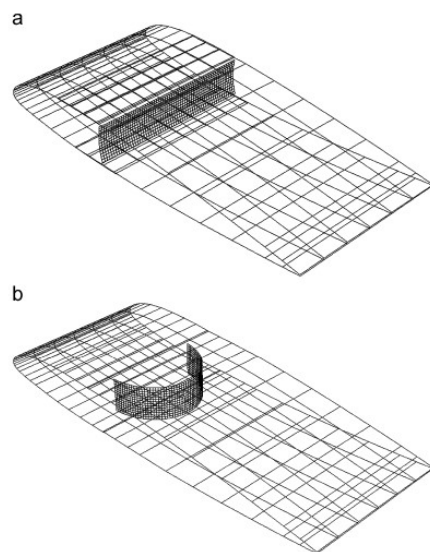


Fig. 6: Isometric view of Chord length morphing

3) Variable sweep wing

Mattioni et al [40] and [39] have modeled a variable-sweep wing with multistable structures whose change in angle reduces the drag and thus plays an important role in the aerodynamics point of view. The outer edges (spar) of the wing are long and straight shells longitudinally with curved cross-sections transversely and are connected by truss ribs. These



(a) straight configuration



(b) deformed or sweep configuration

Fig. 7: Simulation showing the deformation of the sweep wing

curved cross sections give two advantages by providing hinge-like behavior to the spar and also increasing the moment of inertia which is indeed increasing the stiffness and resistance to the bending moment. The structure's initial configuration is straight when it reaches the critical load (critical load is the load at which the bifurcation occurs i.e, the beginning of the buckling of the spar) due to the drag at high speeds, the spar structure shows elastic deformation and buckles, thus behaves like a hinge at the root. Once the load is removed then the structure unfolds and becomes straight. The straight configuration and the deformed configurations are shown in Figure 7a and Figure 7b. The load bearing capability of the considered spars and the ribs are engineered based on the numerical simulation results and experimental results.

4) Sandwich morphing skin

Bubert et al. [3] have developed the aircraft wing span by combining an elastomeric material composite (EMC) to attain one dimensional 100% extension achieved by a 100% increase in surface area. A highly anisotropic material is used which has to run chord-wise and should meet certain requirements: low in-plane actuation, high out-of-plane stiffness and should be able to aerodynamic loads such as carbon fiber reinforcements. For adding the out-of-plane stiffness without affecting the in-plane stiffness a flexible material composite (FMC) has been introduced by Murray et al. [42] that allows large strain in one dimension. To meet the design requirements, a surface layer with a honeycomb structure that exhibits zero-in-plane Poisson's ratio has been used, and to compensate for the bending stiffness, carbon rods are also introduced. But for one-dimensional morphing applications such as chordwise, hindering the Poisson's contraction by constraining would increase the stiffness for actuation in the morphing direction.

So, a zero Poisson's ratio hybrid and accordion honeycombs have been developed by Olympio et al. [45].

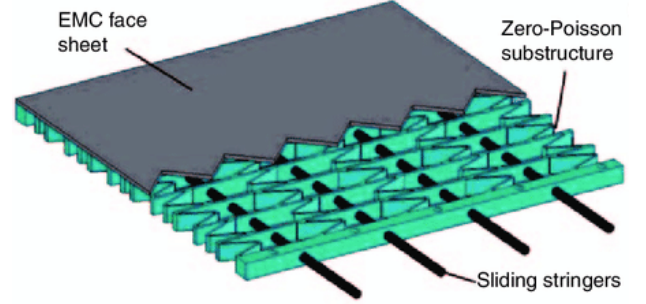


Fig. 8: Flexible matrix composite skin/honeycomb core morphing

5) Curved surface mechanism (CSCFM)

In order to achieve the constant force at the end effector by adjusting the stiffness of the mechanism, Lie et al. [36] used two types of sliders in this mechanism: a curved surface slider that moves along the y-axis and two other sliders that moves in the x-axis in which the curved surface squeezes the sliders with springs along the x-axis whilst moving to and fro along the y-axis by causing a normal force (the schematic representation of working principle is shown in figure Figure 9). The curved surface shape has to be designed carefully because the magnitude and direction of the normal force depend on it, as the contact point is a line contact that is parallel to the z-axis. Forces acting in the system are normal force F_N that is caused at the contact point due to squeezing and is resolved into a horizontal force along the x-axis F_H and a vertical force along the y-axis F_V (friction is ignored for the analysis of the simple model). Using Newton's third law and the resolved components, the following equations are generated and are further used for tracking the path of the curved surface and two followers. To increase the performance of these kinds of mechanisms for increasing output accuracy, CAD/CAM/DNC integration and networked platforms are established.

$$F_V = F_N \cdot \sin\alpha$$

$$F_H = F_N \cos\alpha (F_H = F_s = k \cdot x)$$

where k is the stiffness of the spring and x is the displacement in the x-axis

6) Double slider Mechanism (DSCFM)

In the double slider mechanism is a 1 DOF system in which a pair of sliders with springs are arranged orthogonally as shown in Figure 10. A link with the revolute joint is used to connect these two sliders and is used to transmit the input force to the required constant output force. since the axes are already defined in the schematic figure, Hooke's law is applied by considering x as the input, and y as the output and the following equations were generated.

$$F_x = -k_x \cdot \delta x$$

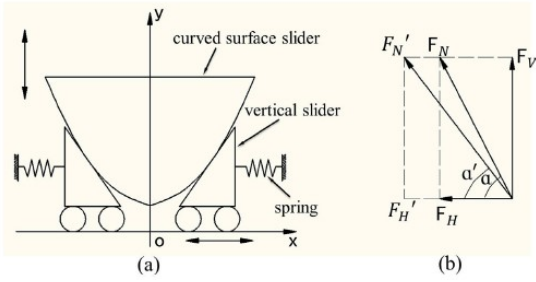


Fig. 9: Simplified model of curved surface constant force mechanism: a) Model b) Resolution of forces

$$F_y = -k_y \cdot \delta y$$

From the power conservation Principle, $\frac{dy}{dx}$ is used in order to map the force of a 1 DOF system from coordinates x to y , and friction is neglected to simplify the model. The following equation has been formed for the given system:

Further, the analysis has been carried out to find the path of the linkage and it is found from the equation ($C_F = K_y \cdot I_y$, where C_F is the curvature) that the link is following an elliptical path which can be formed in an L shape structure. Any 1 Dof system should satisfy the input(x)-output(y) relation. Herder et al. [35] used this concept to design a constant force mechanism of small size with eleven revolute pin joints and two springs to improve the accuracy of the output force.

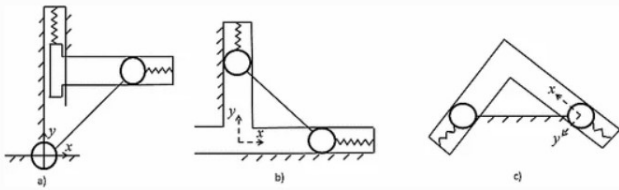


Fig. 10: Three inversions of the double slider constant force mechanisms

7) Stiffness-combined Mechanism design (SCCFM)

The stiffness combined constant force mechanism is the combination of the positive stiffness (reactive force directly proportional to deformation) and negative stiffness (reactive force inversely proportional to deformation) mechanism to achieve a zero stiffness. Positive stiffness is generally achieved by mechanisms that obey Hooke's law, whereas the negative stiffness mechanism is achieved by the bi-stable structures which undergo bifurcation after critical load. Zhao et al. [66, 59] have used this concept of stiffness combination and developed a mechanism by using the magnetic mature system as the negative stiffness structure and the parallel flexure system as the positive stiffness structure for scanning probe where the constant force and highly accurate measurement are important between stylus and workpiece. The schematic representation of the conceptual model of the mechanism

is shown in Figure 11. In this application, the force due to pre-stressed springs, parallel springs, and from the two magnets, armatures combined helps to balance the effect of each other and maintain constant force. The nonlinearity due to the parallel flexure mechanism and the pre-stressed spring are balanced out by using the magnetic force and thus, high accuracy is achieved.

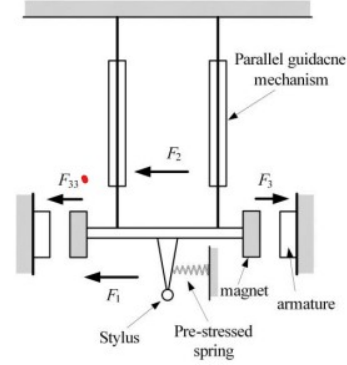


Fig. 11: An application of stiffness combined constant force mechanism

8) Lumped compliance models

From Hou et al. [22] review on CTJMs, a constant torque joint mechanism is the rotational counterpart of the constant force mechanism. A CFM has zero stiffness for certain displacements and the displacement can be changed with the size of the mechanism, whereas the CTJM remains the same irrespective of the size. The CTJM's are classified into two types: 1) Lumped Compliance model which is further divided into three categories (group A, B, and C) 2) Distributed compliance model. Group A of lumped compliance model follows the same concept as the CFM by using the torsion springs for the positive stiffness and the linear springs (From a to c in Figure 12) or torsion spring (Model d in Figure 12) for negative stiffness and their combination forms a zero stiffness mechanism. Group B uses the positive stiffness mechanism and cam mechanism where the design of the cam affects the region of linearity and the schematic model is represented in Figure 13. In Group C, the springs are pre-loaded against the rim or drum in which the joint needs stable frictional force to maintain the constant torque, and the schematic model is represented in Figure 14. The torque-rotation curve doesn't need any pre-load region, these mechanisms depend only on the friction force.

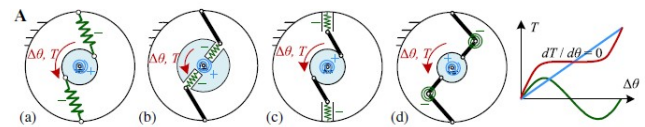


Fig. 12: Lumped compliance of Group A

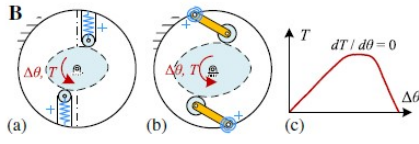


Fig. 13: Lumped compliance of Group B

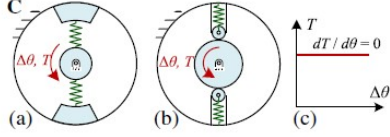


Fig. 14: Lumped compliance of Group C

9) Distributed compliance model

The constant torque in lumped compliance model is obtained by using the linear and torsion spring stiffness at certain locations along the limb whereas from Hampali et al.[21] and Gandhi et al. [16] distributed compliant model the limbs are completely compliant in which the limbs consist of the nature of a linear spring, a torsion spring and the joints used in lumped compliant model by distributing them along the limbs (the schematic representation of the DCM is shown in Figure 15). These models have a very less number of parts compared to the LCM and thus have more torque region. These are of two types based on the shape variation: Type 1 and Type 2. In Type 1, A fully compliant limb connects the inner shaft to the outer rim where the limb is connected into different segments of a certain radius that can be bent and stretched. The radius can be increased to achieve a smoother and larger constant-torque region. In Type 2, the same limb design used in Type 1 can be optimized to improve the mass fabrication of these joints. Despite the simpler geometry, the stress is more in Type 2 because of the less distributed shape. This can be strengthened by reducing the flatness of the limb. Both types eliminate the kinematic joints and reduce the number of parts to assemble. To use this type of model, the size or magnitude of torque can be improved for scaling torque curve and stress curve without optimization by using the following equations.

$$\frac{T \cdot R}{E \cdot I} = Constant$$

$$\frac{\sigma \cdot R}{E \cdot w} = Constant$$

10) Actuator with adjustable stiffness using a lever mechanism

A lever is something that rotates about a pivot point, where Jafari et al. [28] made the lever compliant by adding springs on both sides of the lever by varying the lever arm. The effective arm of the lever is the distance between the springs and the pivot where the stiffness of the lever is adjusted by changing the effective arm length i.e, the position of the spring (AwAS) or the position of the pivot (AwAS 2) as shown in Figure 16 a

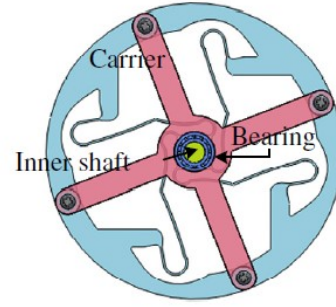


Fig. 15: Distributed compliance Model

& b. Another energy-efficient method from [27] is to adjust the stiffness by changing the point at which the force is applied and the effective arm length in this case is the distance between the point at which the force is applied (compACT VSA) and the pivot as shown in Figure 16. As the stiffness characteristics vary from model to model, an application of each lever concept is shown in Figure 17. The parameters such as the spring stiffness and the lever arm length affect the range of motion and the output force. In [27], a new actuator with the AwAS 2 concept implementation has been developed Figure 17 b which has a wide range of motion and is energy-efficient by consuming less energy based on the elastic element pretension principle.

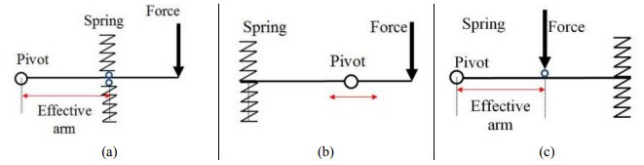


Fig. 16: Actuator with adjustable stiffness using a lever mechanism a) AwAS b) AwAS 2 c) compACT VSA

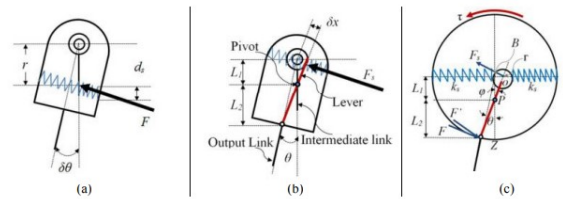


Fig. 17: Application of lever mechanism with a) AwAS b) AwAS 2 c) compACT VSA

Similarly, an application of the AwAS concept is developed by Jafari et al. [29] and the conceptual model of this new actuator is shown in Figure 18. In all these applications motors are used for varying the effective arm lengths.

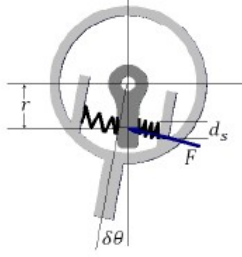


Fig. 18: Application of lever mechanism with AwAS

11) Statically balancing a reconfigurable mechanism

When the potential energy of the mechanism remains constant at all the positions then the mechanism is said to be statically balanced. Tseng et al. [56] have explained a mechanism with 1 DOF reconfigurable linkage as shown in Figure 19 that is statically balanced by two individual springs and the balance can be achieved by eliminating the gravity. And another model by Kuo et al.[33] for the same 1 DOF reconfigurable linkage consists of only one passive energy element and is perfectly balanced, where the passive element could be a counterweight or a spring with the analytical results and experimental studies. In the model shown in Figure 20, the mechanism is statically balanced by adding 2 zero free-length (ZFL) springs that can articulate between the links and these virtual ZFL springs can be replaced by one real spring: formed by using a wired pulley system. Meanwhile, there are some factors that may result in this imperfect balancing, for example friction and backlash at joints and pulleys, the non-linearity of spring stiffness, actual parameters of the pulleys, hysteresis, and manufacturing tolerances of the links.

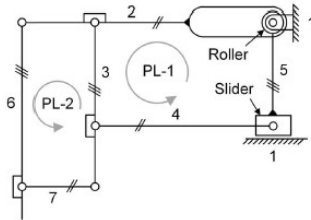


Fig. 19: Reconfigurable mechanism model

12) Rotational cam-based VSA

In an antagonistic VSA, the articulation becomes stiffer with respect to the increase in antagonistic forces. The stiffness is adjusted with the help of the non-linear elastic element. Using the concept of Antagonistic variable stiffness actuator [26, 20] and linear WWC-VSA by Spagnuolo et al. in [53] which has an infinite range of linear motion theoretically, a Rotational WWC-VSA has been developed that has an exceptional range of motion to actuate with no restrictions and able to perform infinite turns but this has to be constrained to perform a certain limited range of motions rotational operations. The schematic representation of the conceptual model in Figure 21 has a

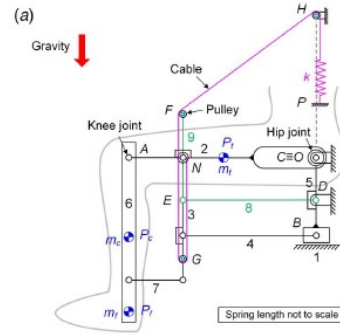


Fig. 20: Application of Reconfigurable mechanism in rehabilitation

cam that is used for wrapping the wire in order to decrease the number of components and limit the mechanical stresses, a tension spring, and a wire. In RWWC-VSA, the free end of the wire is fixed about the center of the cam that is fixed with respect to the frame of reference and rotates with it. Some geometric conditions have to be fulfilled for the functioning of the actuator, such as

$$A\vec{E}^0 \geq w_{min} + l^0_l$$

$$d(O_c, \vec{V}E) > r_b + \frac{d_{t,max}}{2}$$

Note: The reference figure for the above equation is Figure 21

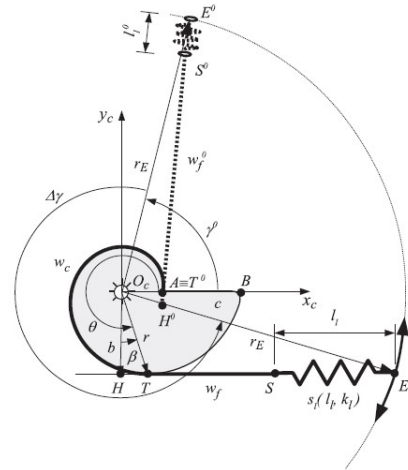


Fig. 21: Conceptual model of RWWC-VSA

RWWC-VSA has been represented in Figure 22. By reducing the overall dimensions or by modifying the range of motion, there is a chance to employ the multi-turn spiral cams.

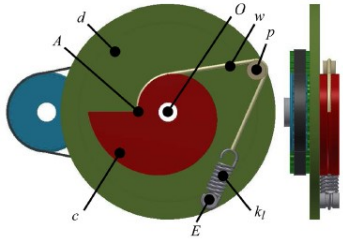


Fig. 22: An application of RWVC-VSA

13) Floating Spring Joint (FSJ)

wolf et al. [62] developed this semi-active 1 DOF joint with the intention to make it energy efficient, and low friction and to use the maximum potential energy of the spring without the loss due to the pretension of the spring to achieve the desired torque. FSJ is derived from the VS-joint by Wolf et al. [63] and QA-joint by Eiberger et al. [13], which adds the advantage to the range of stiffness. The joint has a spring surrounded by a non-linear and active adjustment system with 2 cam disks. Spring is not attached to any of the housing but superimpose the cam disks together. By using rollers, one of the cam disks is used for adjusting the stiffness while the other supported the output base which has both axial and radial motion. There is a passive joint deflection (spring deflection) that pushes the cam disks apart with an axial displacement without interacting with the housing while increasing the stiffness. This generates two torques as the force applied has two different directions and thus, the joint is energy efficient and compact since there is only one spring. The schematic representation of the conceptual model of FSJ is in Figure 23

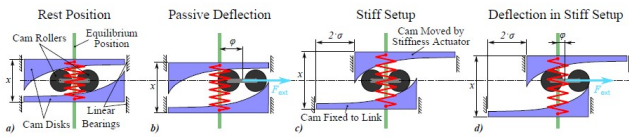


Fig. 23: Conceptual model of Floating Spring Joint: a) Initial configuration b) an external torque is applied results in passive deflection c) In equilibrium position with stiffness preset d) system in stiff preset with external load applied.

In VS-joint the torque is generated by the cam disk and roller, where the rotational joint deflection causes the axial displacement of the spring as shown in Figure 24. In QS-Joint the output torque is generated by two cam disks by squeezing the spring elements (single spring connected to the rollers that are in contact with cam discs). These are of two types and the schematic model of the concepts is shown in Figure 25 a & b.

14) Adapted triangle mechanism

Tonietti et al. [55] presented a conceptual model of a variable stiffness actuator as shown in Figure 26 that could control the joint position and stiffness of the mechanism. A transmission

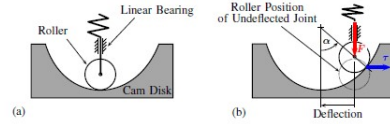


Fig. 24: Variable stiffness (VS) joint With a) Initial configuration b) Deflected position

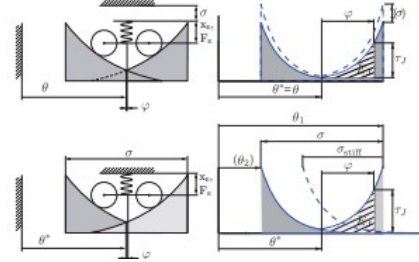


Fig. 25: Quasi-Antagonistic (QA) joint with a) Preload variable type b) Transmission variable type

belt (Non-linear elastic element) is tensioned by a linear spring that non-linearly connects the main shaft and the antagonistic actuators that are rigidly connected to the motors. The pre-stressed tension spring pushes the tendon creating non-linearity and thus, forms a triangle where the height of the triangle determines the stiffness of the mechanism. The height of this triangle relative to half the base length determines the stiffness of the mechanism. In this way, the stiffness of the mechanism can be varied rapidly and continuously during the transmission. The simplified model for the adapted triangle mechanism is shown in Figure 27, used in bionics for finger movement by Markus et al. [17]. The only difference in this mechanism from the conceptual model is, the winder shown in the picture is the only antagonistic pulley that acts as a first pulley.

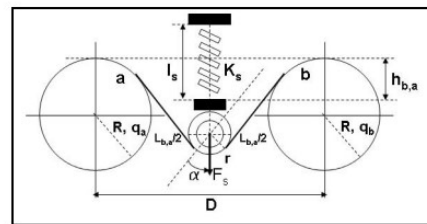


Fig. 26: Set up of the non-linear spring element

15) Discrete layer jamming

Zhou et al. [68] have presented the discrete layer jamming that has a series of layered beams whose stiffness is varied by the pressure clamps placed along the beam as shown in Figure 28. Changing the position of the clamps or the number of clamps or clamp pressure and coefficient of friction increases the friction between the layers, and hence, the bending stiffness of the beam increases. A continuous layer

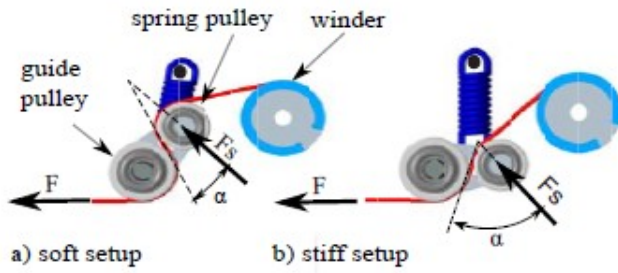


Fig. 27: Antagonistic drive compliant mechanism

jamming with pneumatic and hydraulic systems might have a leakage issue but there is no such problem in the discrete layer jamming model. Additionally, this mechanism doesn't need any elastomeric membrane on the surface to avoid damage from contacts with sharp edges.

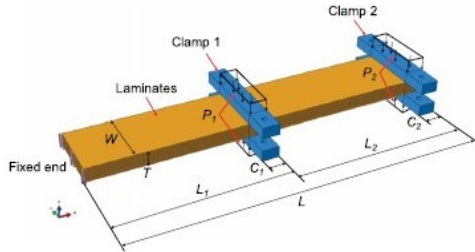


Fig. 28: Simplified model of the discrete layer jamming system

16) Disc spring

Chen et al. [6] designed a PNSJ with low-frequency vibration isolation. The geometrical parameters and structural characteristics were made according to the Euler beam theory, in order to change the stiffness of the system. The contact supports are not restricted to the x and y axes but provide the restoring force within a cone (initial position). The leaf spring is used as the flexural Euler beam structure and obtains low stiffness in the horizontal direction while achieving negative stiffness in the vertical direction. A Non-linear disc spring is used for the large load-bearing capacity and low stiffness in the vertical direction which is connected to the bucked leaf spring in order to provide the dynamics stiffness (the leaf spring and the dick spring are attached in parallel at the equilibrium point) and thus, isolating the frequency from the system in multiple directions. The schematic representation of the system is shown in Figure 29. This concept applies to medical rehabilitation exoskeletons, high-precision surgical tools, etc.

B. Results

From section II, it has been realized that there are only a few conceptual solutions that can be applicable for wrist

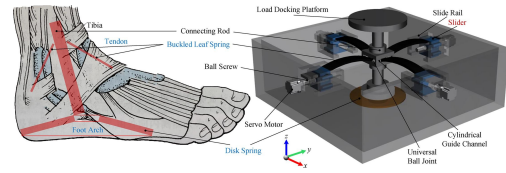


Fig. 29: Bionic model of a variable stiffness vibration isolated joint

support for weight compensation and stiffness compensation. The concepts mentioned in the previous section have passive and semi-passive mechanisms used in different applications and during the categorization of these mechanisms based on their working principle. Firstly, stiffness variation based on material property change involves the use of some external energy source such as heat energy [49] and magnetic field [67] whereas in the case of mechanisms that come under the boundary conditions category, despite having semi-active mechanisms they do have some delay in the stiffness variation [64]. Although the mechanisms in structural and preload are active, from section II it is found that the passive and semi-passive mechanisms were achieved by structural or shape morphing (changing the moment of inertia) and by giving preload to the springs. So, from the study on working principle, a new categorization for the mechanisms that can be used has been made as a flow chart and is shown in Figure 30.

Following the new categorization mentioned in Figure 30 and the concepts studied in section II, one of the applications of these mechanisms along with the advantages and disadvantages of the mechanism, are tabulated in Table II. Later, a comparison and evaluation of these mechanisms have been performed on these mechanisms as shown in Table II, considering certain parameters such as weight, size, stiffness, and adaptability of the concept with the wrist considering the weight and size. As the mechanism is going to be on the wrist, the weight of the stiffness should be as less as possible, while the size of the mechanism should also be small as the large size mechanisms are difficult to fit in the limited space, moreover, large mechanisms hinder the movements of the arm supports. The stiffness has to be sufficient enough to compensate for the weight and stiffness, also the described mechanism has to be adaptable in the development of wrist orthoses. The rating is given from 1 to 5 for each parameter depending on the size (1 to 5 has been given based on the number of parts), weight, and stiffness (1 above 100, 2 above 20, 3 above 10, 4 above 4 and 5 below 4) of the mechanism while adaptability is the sum of the grade of the weight and size (since adaptability depends on the size and weight). So, a good rating has been given to the mechanism with a small size, less weight, required stiffness, and adaptability in design considering the size and weight. The results from the table are further discussed in section III section.

Rating		Stiffness
1	Very likely	≥ 100
2	Likely	$\geq 20, < 100$
3	Applicable	$\geq 10, < 20$
4	Barely	$\geq 4, < 10$
5	Not likely	< 4

TABLE I: Description of the rating and the rating given for the stiffness range

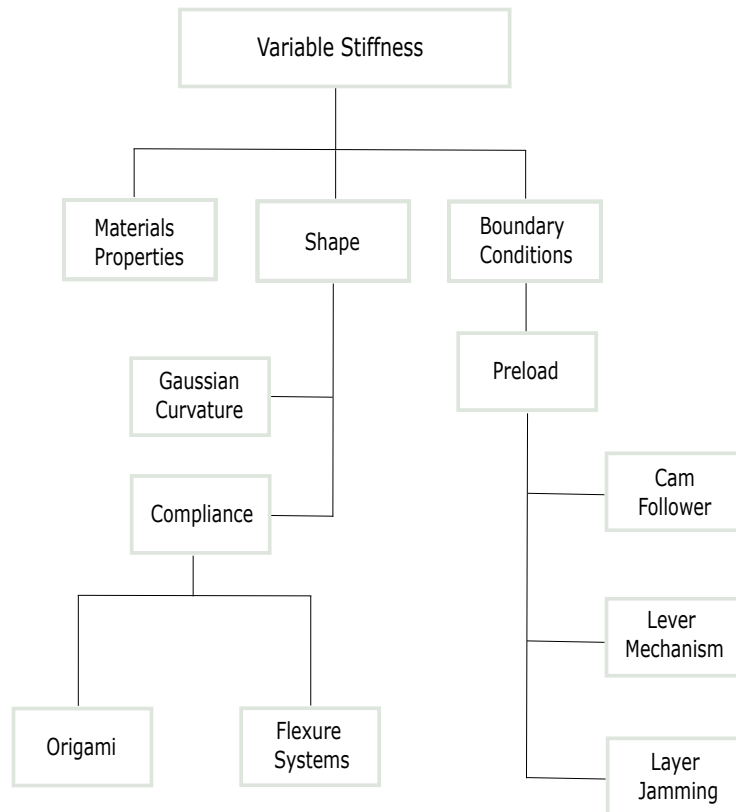


Fig. 30: Flow chart based on the literature from [section II](#)

TABLE II: ADVANTAGES AND DISADVANTAGES OF DIFFERENT MECHANISMS BASED ON THE DISCUSSED CATEGORIZATION

Note: The advantages and disadvantages are not presented based on application but in the general overview of the mechanisms

Category	Concept	Application	Advantages	Disadvantages	DOF	Number of Parts	Rating						Reference
							Stiffness ratio (Max/Min)	Size	Weight	Stiffness	Adaptability (Size*weight)	Final Score (Stiffness + Adaptability)	
Gaussian curvature shells	Tri-stable structure	Airfoil morphing	Simple model, Small size	Low stiffness	2	4	Not specified	5	2	4	10	14	[38, 23, 24, 25]
	Bi-stable flap design	Aircraft wing	High stiffness	Low displacement, Occupies More space	1	>3	Not specified	4	3	3	12	15	[8]
	Variable sweep wing	Trailing edge	High Stiffness, Decent range of motion	Large size, Complicated to design, Difficult to manufacture	2	>6	Not specified	5	3	2	15	17	[40, 39]
Origami	Sandwich morphing skin	Spanwise wing shape in aircraft	Scalable from micro to meter scale, Can be self-actuated without-external actuators and Easy to manufacture	Complex modeling, Difficult to extend to more degrees of freedom	1	2	44.9	5	2	3	10	13	[42, 3]
Cam-follower	Curved surface constant force	Industrial Applications-Object holding, grinding	Large constant-force stroke, Compact structure, Good loading distribution, Simple mathematical model	Low output accuracy, Difficulty in machining, Triangular notch in the working surface	1	4	40.6	5	4	2	8	10	[36]
	Lumped compliance models	Knee, Ankle exoskeleton	Good range of motion, Sufficient stiffness variation	Suffering from natural defects of conventional technologies, Low output accuracy	1	8	5	3	2	3	6	9	[22]
	Floating Spring Joint	DLR Hand arm	Can be mounted away from-the balanced joint, Adjustment through either-cam shape or spring properties, Low profile mechanism	Complex cam design	2	5	10	3	3	3	9	12	[62, 63, 13]
	Rotational cam-based VSJ	Hammering, holding cups, and drumming	Low profile mechanism, Can be mounted away from-the balanced joint and-adjustment through either-cam shape or spring properties	Complex cam design	2	4	4.9	4	5	3	20	23	[26, 20, 53]
Lever Mechanisms	Double slider constant force	Revolute joint	Simple structure, Simple machining technology, High interchangeability	Suffering from friction, wear and backlash, large output error	1	6	1.34	4	3	5	12	17	[35]
	Actuator with adjustable stiffness using a lever mechanism	Prosthetics for lower limbs	Adjustment through either-cam-follower shape or-spring properties, Low profile mechanism	Friction influences balancing, More wear	1	>4	43.33	4	3	1	12	13	[28, 27]
	Adapted triangle mechanism	Bionics and legged robots	Fast and safe operation, High accuracy, compact in size, Capable of independently-varying the stiffness-and main shaft position	Needs high friction, constant spring load is needed on the tendon	1	5	500	4	4	1	16	17	[55, 17]
	Statically balancing a reconfigurable mechanism	Knee and Hip exoskeleton	Easy to model, Less weight	Links can buckle over time, Friction at the joints	1	9	3.8	5	2	4	10	14	[56, 33]
Flexure systems	Stiffness combined mechanism design	Silicon micromachining	High output accuracy, Simple structure, No wear, No backlash, and no friction, Low requirement for material, Reduce driving force	Be sensitive to the parameters, High requirement of manufacture, Complicated mathematical model, Small constant-force stroke	1	>=4	1	3	5	5	15	20	[66, 59]
	Distributed compliance model	Knee, Ankle exoskeleton	Compact size, Large constant-force stroke, High output accuracy, Complicated design	Suffering from natural defects of -conventional technologies, Low output accuracy	1	2	10	3	2	3	6	9	[21, 16]
	Disc spring	Ankle joint	Simple mechanism, Limited parts required	Small displacement	1	2	100	4	2	2	8	10	[6]
Layer Jamming	Discrete layer jamming	Co-robots	High stiffness variation in-small sizes, Compact	Clamping need high pressure	1	>5	17	3	3	3	9	12	[68]

III. DISCUSSION

The aim of this review was to find the variable stiffness mechanism that can compensate for the weight of the hand and stiffness. So, based on the concepts described in the [section II](#), in [subsection II-B](#) section, the sub-categorization of each of the categories has been made and has been mentioned in the flow chart [Figure 2](#). Each of the mechanisms has its own application, and accordingly, they have advantages and disadvantages. In the [Table II](#), the advantages and disadvantages are presented from a general point of view but not for the specific application. However, the table is still incomplete as there are many of the unmentioned applications related to either the wrist support or the exoskeleton. Although there are other pros and cons to these mechanisms, in order to make this more general, only common points are presented but the mentioned points are important.

From the literature study, it has been realized that there are limited resources for weight or stiffness compensation of wrist support. Following [Table I](#), in the next table, the concepts found in the [section II](#) are evaluated based on the performance parameters. Based on the evaluation and the final rating, the concept is finalized but the ratings presented in the table are given based on human instincts. For instance, the rating of the weight is given based on the number of parts and similarly, the rating of the size is given depending on the application of the concept and the number of parts in the conceptual model of that particular application. Since these two ratings (size and weight) depend on adaptability, the final score is affected. The comparison provided global insights into design properties. The mechanisms with the lowest performance score shall be shortlisted and can further be used for the development of wrist support in the research. From the literature review, it has been realized that the shortlisted mechanism has been a semi-active mechanism in which the stiffness is changed using an active element. This active element will be made passive during the research besides the development of the zero stiffness mechanism for stable equilibrium position using the evaluated concept.

There are some limitations in this review. Firstly, the mechanisms studied and described in the review are completely passive and semi-active. As there are limited articles and applications of passive systems on wrist and hand exoskeletons, it was decided to develop a passive system. In fact, active systems can also be used, but an external energy source is needed to use them which makes the user use them for a limited time. Moreover, batteries are needed to provide energy, and this makes the device heavy. Thus, the requirement for batteries is a limitation to use the active system. Secondly, the categorization names used in the review are regularly used mechanical transmission systems. For instance, cam-follower is the sub-category of the preload but this is a conflict with other cam-follower mechanisms. There are a few variable stiffness mechanisms that can be achieved using the cam follower principle, since these fall under the cam-follower

category, they were named after that. Finally, all the described concepts are few among the many available variable stiffness concepts.

IV. CONCLUSION

The aim of this review is to find a passive and semi-active variable stiffness mechanism that can be used in wrist support. To find this, categorization has been made among the concepts found in the literature study. Further, the mechanisms found were studied in depth and the sub-categorization has been made based on the working principle of each of the mechanisms. Each of the mechanisms' applications, advantages, and disadvantages are presented. Followed by an evaluation of each of them based on the parameters: size, weight, stiffness, and adaptability. The concepts that have the lowest score between certain ranges are chosen for the development of wrist support.

Overall, it is realized that the excessive use of orthoses might progress the disease and the device requirement depends on the type of disease and the progression of the disease. There are a limited number of devices available for wrist support and are in research phase. These devices work only in specific orientations or for specific functions and are also very bulky and heavy which makes them less applicable. In addition, some commercially available devices can function in specific orientations only.

Future work can be focused on universal scoring factors to evaluate and compare the performance of the concepts in literature, which could help in presenting a more refined overview of performance for those seeking to use variable stiffness concepts in new applications. Also, each of these concepts is evaluated for a limited number of articles which is supposed to be done for a large number of articles.

REFERENCES

- [1] Andres F Arrieta et al. "Dynamic control for morphing of bi-stable composites". In: *Journal of Intelligent Material Systems and Structures* 24.3 (2013), pp. 266–273.
- [2] Samira Azizi, Kaveh Karami, and Satish Nagarajaiah. "Developing a semi-active adjustable stiffness device using integrated damage tracking and adaptive stiffness mechanism". In: *Engineering Structures* 238 (2021), p. 112036.
- [3] Edward A Bubert et al. "Design and fabrication of a passive 1D morphing aircraft skin". In: *Journal of intelligent material systems and structures* 21.17 (2010), pp. 1699–1717.
- [4] Federico Carpi et al. "Enabling variable-stiffness hand rehabilitation orthoses with dielectric elastomer transducers". In: *Medical engineering & physics* 36.2 (2014), pp. 205–211.
- [5] Handdeut Chang, Sangjoon J Kim, and Jung Kim. "Development of active stiffness mechanism for self-stabilizing manipulator". In: *2016 16th International Conference on Control, Automation and Systems (IC-CAS)*. IEEE. 2016, pp. 912–917.

- [6] Renzhen Chen et al. “A variable positive-negative stiffness joint with low frequency vibration isolation performance”. In: *Measurement* 185 (2021), p. 110046.
- [7] Fuhong Dai, Hao Li, and Shanyi Du. “Design and analysis of a tri-stable structure based on bi-stable laminates”. In: *Composites Part A: Applied Science and Manufacturing* 43.9 (2012), pp. 1497–1504.
- [8] Stephen Daynes, PM Weaver, and KD Potter. “Aeroelastic study of bistable composite airfoils”. In: *Journal of aircraft* 46.6 (2009), pp. 2169–2174.
- [9] Cezar Diaconu, Paul Weaver, and Filippo Mattioli. “Solutions for morphing airfoil sections using bi-stable laminated composite structures”. In: *48th AIAA/ASME/ASCE/AHS/ASC Structures, Structural Dynamics, and Materials Conference*. 2007, p. 1719.
- [10] Cezar G Diaconu, Paul M Weaver, and Filippo Mattioli. “Concepts for morphing airfoil sections using bi-stable laminated composite structures”. In: *Thin-Walled Structures* 46.6 (2008), pp. 689–701.
- [11] Aaron M Dollar and Hugh Herr. “Lower extremity exoskeletons and active orthoses: Challenges and state-of-the-art”. In: *IEEE Transactions on robotics* 24.1 (2008), pp. 144–158.
- [12] Joseph Dooley et al. “Duchenne muscular dystrophy: a 30-year population-based incidence study”. In: *Clinical pediatrics* 49.2 (2010), pp. 177–179.
- [13] Oliver Eiberger et al. “On joint design with intrinsic variable compliance: Derivation of the DLR QA-joint”. In: *2010 IEEE International Conference on Robotics and Automation*. IEEE. 2010, pp. 1687–1694.
- [14] Alan EH Emery. “Population frequencies of inherited neuromuscular diseases—a world survey”. In: *Neuromuscular disorders* 1.1 (1991), pp. 19–29.
- [15] Daniel P Ferris and W Sebastian Barrutia. “Novel Designs for Passive Elastic Lower Limb Exoskeletons”. In: *International Symposium on Wearable Robotics*. Springer. 2020, pp. 27–31.
- [16] Ishit Gandhi and Hong Zhou. “Synthesizing constant torque compliant mechanisms using precompressed beams”. In: *Journal of Mechanical Design* 141.1 (2019).
- [17] Markus Grebenstein et al. “The DLR hand arm system”. In: *2011 IEEE International Conference on Robotics and Automation*. IEEE. 2011, pp. 3175–3182.
- [18] Xinyu Guan, Linhong Ji, and Rencheng Wang. “Development of exoskeletons and applications on rehabilitation”. In: *MATEC Web of Conferences*. Vol. 40. EDP Sciences. 2016, p. 02004.
- [19] Muhammad Ahsan Gull, Shaoping Bai, and Thomas Bak. “A review on design of upper limb exoskeletons”. In: *Robotics* 9.1 (2020), p. 16.
- [20] Ronald van Ham et al. “Compliant actuator designs”. In: *IEEE Robotics & Automation Magazine* 3.16 (2009), pp. 81–94.
- [21] Shamanth Hampali, Anoosha Pai S, and GK Ananthasuresh. “A Tunable Variable-Torque Compliant Hinge Using Open-Section Shells”. In: *Journal of Mechanisms and Robotics* 12.6 (2020).
- [22] Chia-Wen Hou and Chao-Chieh Lan. “Functional joint mechanisms with constant-torque outputs”. In: *Mechanism and Machine Theory* 62 (2013), pp. 166–181.
- [23] Michael W Hyer. “Calculations of the room-temperature shapes of unsymmetric laminates two”. In: *Journal of Composite Materials* 15.4 (1981), pp. 296–310.
- [24] Michael W Hyer. “Some observations on the cured shape of thin unsymmetric laminates”. In: *Journal of Composite Materials* 15.2 (1981), pp. 175–194.
- [25] Michael W Hyer. “The room-temperature shapes of four-layer unsymmetric cross-ply laminates”. In: *Journal of Composite Materials* 16.4 (1982), pp. 318–340.
- [26] Amir Jafari. “Coupling between the output force and stiffness in different variable stiffness actuators”. In: *Actuators*. Vol. 3. 3. MDPI. 2014, pp. 270–284.
- [27] Amir Jafari, Nikos Tsagarakis, and Darwin Caldwell. “Energy efficient actuators with adjustable stiffness: a review on AwAS, AwAS-II and CompACT VSA changing stiffness based on lever mechanism”. In: *Industrial Robot: An International Journal* (2015).
- [28] Amir Jafari, Nikos G Tsagarakis, and Darwin G Caldwell. “AwAS-II: A new actuator with adjustable stiffness based on the novel principle of the adaptable pivot point and variable lever ratio”. In: *2011 IEEE International Conference on Robotics and Automation*. IEEE. 2011, pp. 4638–4643.
- [29] Amir Jafari et al. “A novel actuator with adjustable stiffness (AwAS)”. In: *2010 IEEE/RSJ International Conference on Intelligent Robots and Systems*. IEEE. 2010, pp. 4201–4206.
- [30] Mariska MHP Janssen et al. “Dynamic arm study: quantitative description of upper extremity function and activity of boys and men with duchenne muscular dystrophy”. In: *Journal of neuroengineering and rehabilitation* 14.1 (2017), pp. 1–14.
- [31] Didu Kariyawasam et al. “Incidence of Duchenne muscular dystrophy in the modern era; an Australian study”. In: *European Journal of Human Genetics* (2022), pp. 1–7.
- [32] Izabela K Kuder et al. “Variable stiffness material and structural concepts for morphing applications”. In: *Progress in Aerospace Sciences* 63 (2013), pp. 33–55.
- [33] Chin-Hsing Kuo et al. “Statically balancing a reconfigurable mechanism by using one passive energy element only: a case study”. In: *Journal of Mechanisms and Robotics* 13.4 (2021).
- [34] Pei-Hsin Kuo and Ashish D Deshpande. “Novel design of a passive variable stiffness joint mechanism: Inspiration from biomechanics of hand joints”. In: *Dynamic Systems and Control Conference*. Vol. 56130. American Society of Mechanical Engineers. 2013, V002T28A003.
- [35] Patrice Lambert and Just L Herder. “An adjustable constant force mechanism using pin joints and springs”.

- In: *New trends in mechanism and machine science*. Springer, 2017, pp. 453–461.
- [36] Yang Liu et al. “Design of a curved surface constant force mechanism”. In: *Mechanics Based Design of Structures and Machines* 45.2 (2017), pp. 160–172.
- [37] Fabiana Luisa Mattar and Claudia Sobreira. “Hand weakness in Duchenne muscular dystrophy and its relation to physical disability”. In: *Neuromuscular Disorders* 18.3 (2008), pp. 193–198.
- [38] F Mattioni, Paul M Weaver, and MI Friswell. “Multi-stable composite plates with piecewise variation of lay-up in the planform”. In: *International Journal of Solids and Structures* 46.1 (2009), pp. 151–164.
- [39] Filippo Mattioni. “Thermally induced multi-stable composites for morphing aircraft applications”. PhD thesis. University of Bristol, 2009.
- [40] Filippo Mattioni et al. “The application of residual stress tailoring of snap-through composites for variable sweep wings”. In: *47th AIAA/ASME/ASCE/AHS/ASC structures, structural dynamics, and materials conference 14th AIAA/ASME/AHS adaptive structures conference 7th*. 2006, p. 1972.
- [41] Craig M McDonald et al. “Profiles of neuromuscular diseases. Duchenne muscular dystrophy.” In: *American journal of physical medicine & rehabilitation* 74.5 Suppl (1995), S70–92.
- [42] Gabriel Murray, Farhan Gandhi, and Charles Bakis. “Flexible matrix composite skins for one-dimensional wing morphing”. In: *Journal of Intelligent Material Systems and Structures* 21.17 (2010), pp. 1771–1781.
- [43] Ali Amoozandeh Nobaveh and Brandon Caasbrood. “Design Feasibility of an Energy-efficient Wrist Flexion-Extension Exoskeleton using Compliant Beams and Soft Actuators”. In: *2022 International Conference on Rehabilitation Robotics (ICORR)*. IEEE. 2022, pp. 1–6.
- [44] Marcos B Oliveira et al. “Design of a variable stiffness wrist brace with an origami structural element”. In: *Smart Materials, Adaptive Structures and Intelligent Systems*. Vol. 51951. American Society of Mechanical Engineers. 2018, V002T08A009.
- [45] Kingnidé Raymond Olympio and Farhan Gandhi. “Zero Poisson’s ratio cellular honeycombs for flex skins undergoing one-dimensional morphing”. In: *Journal of intelligent material systems and structures* 21.17 (2010), pp. 1737–1753.
- [46] Tadej Petrič et al. “Assistive arm-exoskeleton control based on human muscular manipulability”. In: *Frontiers in neurorobotics* 13 (2019), p. 30.
- [47] Tiaan du Plessis, Karim Djouani, and Christiaan Oosthuizen. “A review of active hand exoskeletons for rehabilitation and assistance”. In: *Robotics* 10.1 (2021), p. 40.
- [48] Tommaso Poliero et al. “Applicability of an active back-support exoskeleton to carrying activities”. In: *Frontiers in Robotics and AI* 7 (2020), p. 579963.
- [49] Wolfram Raither, Andrea Bergamini, and Paolo Ermanni. “Profile beams with adaptive bending–twist coupling by adjustable shear centre location”. In: *Journal of intelligent material systems and structures* 24.3 (2013), pp. 334–346.
- [50] Oscar Sandoval-Gonzalez et al. “Design and development of a hand exoskeleton robot for active and passive rehabilitation”. In: *International Journal of Advanced Robotic Systems* 13.2 (2016), p. 66.
- [51] Marc R Schultz. “A concept for airfoil-like active bistable twisting structures”. In: *Journal of Intelligent Material Systems and Structures* 19.2 (2008), pp. 157–169.
- [52] Andre Seyfarth. “Passive Compliance in Legged Systems and Assistive Devices”. In: *International Symposium on Wearable Robotics*. Springer. 2020, pp. 33–37.
- [53] G Spagnuolo et al. “Analysis and synthesis of LinWWC-VSA, a Variable Stiffness Actuator for linear motion”. In: *Mechanism and Machine Theory* 110 (2017), pp. 85–99.
- [54] Hideo Sugita and Shin’ichi TAKEDA. “Progress in muscular dystrophy research with special emphasis on gene therapy”. In: *Proceedings of the Japan Academy, Series B* 86.7 (2010), pp. 748–756.
- [55] Giovanni Tonietti, Riccardo Schiavi, and Antonio Bichi. “Design and control of a variable stiffness actuator for safe and fast physical human/robot interaction”. In: *Proceedings of the 2005 IEEE international conference on robotics and automation*. IEEE. 2005, pp. 526–531.
- [56] Tzu-Yu Tseng et al. “A novel reconfigurable gravity balancer for lower-limb rehabilitation with switchable hip/knee-only exercise”. In: *Journal of Mechanisms and Robotics* 9.4 (2017), p. 041002.
- [57] Loek A Van der Heide et al. “An overview and categorization of dynamic arm supports for people with decreased arm function”. In: *Prosthetics and orthotics international* 38.4 (2014), pp. 287–302.
- [58] Marilyn B Wagner, Paul J Vignos Jr, and Chris Carlozzi. “Duchenne muscular dystrophy: a study of wrist and hand function”. In: *Muscle & Nerve: Official Journal of the American Association of Electrodiagnostic Medicine* 12.3 (1989), pp. 236–244.
- [59] Hongxi Wang et al. “A novel constant-force scanning probe incorporating mechanical-magnetic coupled structures”. In: *Review of Scientific Instruments* 82.7 (2011), p. 075101.
- [60] Piyu Wang and Qingsong Xu. “Design and modeling of constant-force mechanisms: A survey”. In: *Mechanism and Machine Theory* 119 (2018), pp. 1–21.
- [61] Ren-Jeng Wang and Han-Pang Huang. “An active-passive variable stiffness elastic actuator for safety robot systems”. In: *2010 IEEE/RSJ International Conference on Intelligent Robots and Systems*. IEEE. 2010, pp. 3664–3669.
- [62] Sebastian Wolf, Oliver Eiberger, and Gerd Hirzinger. “The DLR FSJ: Energy based design of a variable stiff-

3

Research Paper

Constant Torque Mechanism for Gravity Balancing in Wrist Support Application

Dhanush Chitluri (5481031)
Department of Precision and Microsystems Engineering
Delft University of Technology
Delft, The Netherlands
D.chitluri@student.tudelft.nl

Abstract—Individuals suffering from neuromuscular conditions, such as Duchenne muscular dystrophy (DMD), experience progressive weakening of muscles. Consequently, they require supporting devices like orthoses or exoskeletons to perform daily activities. Although immense efforts are put into developing exoskeletons, limited wrist support devices are available. This is due to the torque variation with the hand's position. The existing wrist orthoses can counteract gravitational forces and support their hands but often utilise rigid body mechanisms or active power sources, which come with drawbacks, including bulkiness and discomfort. This paper proposes an innovative passive wrist support orthoses design based on a compliant mechanism to address these limitations. Our design focuses on supporting a single degree of freedom in hand movements, particularly flexion and extension. By employing parametric optimization, we developed a compliant mechanism that efficiently compensates for the weight of the hand against gravity. The resulting compliant mechanism design is safe, compact, and lightweight, making it an ideal solution for supporting the wrist's degrees of freedom and for applying the device. To validate our design, we conducted experimental testing, comparing the results with the analytical model. Through the experimental validation of the model, the results are interpreted as the mechanism's usefulness in wrist flexion and extension support. In short, our research demonstrates the effectiveness of using compliant mechanisms in wrist support orthoses, especially for individuals with neuromuscular conditions like DMD.

Index Terms—Duchenne muscular dystrophy (DMD), constant torque, wrist support, orthoses/ exoskeleton.

I. INTRODUCTION

Muscular disorders are a group of genetic conditions that profoundly impact individuals' lives. These disorders arise from genetic mutations affecting specific muscle groups, leading to various degrees of muscle weakness and dysfunction. One commonly inherited muscular disorder is Duchenne muscular dystrophy (DMD), which predominantly affects male children [12]. DMD is caused by a mutation in specific genes, resulting in the lack of a protein in muscle fibers. This disease is characterized by progressive muscle fiber damage with the person's age, which begins in the lower limbs and gradually extends to the upper limbs. As the disorder advances, it affects muscle strength and stiffness, causing significant physical limitations and mobility challenges for affected individuals. Individuals affected by DMD pose considerable difficulties in performing daily tasks and activities and, thus, impact the quality of life.

To improve the quality of life for individuals affected by muscular disorders, assistive devices such as orthoses and exoskeletons are employed to provide support. These wearable devices serve the dual purpose of restoring functionality and providing much-needed support. While these devices are extensively used in rehabilitation settings, they also have applications in industrial contexts [17]. Numerous exoskeletons have been researched and developed to aid patients with lower limb [14] and upper limb [6] [38] impairments. However, it is evident from the existing literature that there are limited exoskeletons available for hand support, out of which some of them are actively and semi-actively stimulated supports, which makes the device bulky, uncomfortable, and can hinder the natural movements[13].

To address the limitations associated with active and semi-active exoskeletons, implementing a passive exoskeleton has become imperative to provide effective hand support. Hasegawa et al. [15] developed a passive counterweight balancing mechanism to compensate for the hand weight, thereby reducing the loading on the wrist during desk-based activities. Bas et al. [4] has developed a constant torque gravity compensation for the hand with the constant force mechanism and some other similar passive wrist supports that are available [1], [11]. Despite the current endeavors in passive gravity balancing supports, these devices typically consist of numerous joints, leading to increased friction and bulkiness due to multiple components. Consequently, users often experience discomfort when using such systems.

To overcome these problems, Compliant mechanisms (CM) can be used for developing balancing mechanisms. These mechanisms offer several advantages over traditional rigid-body mechanisms. By incorporating the bending and flexing of slender segments within their components, compliant mechanisms achieve their intended purpose with fewer moving parts and reduced wear. By minimizing the number of parts and integrating the compliant features directly into the design, CMs offer enhanced accuracy and reliability, unlike some devices based on rigid body mechanisms that often rely on sensors [25], actuators [35], and complex control systems [34] to maintain constant torque. CMs provide a simple and efficient solution without the need for extensive electronic components and thus, have widespread applications in industrial and med-

ical devices, as well as everyday products[20], [19], [31]. Amoozandeh et al.[2] developed passive wrist support with a compliant spatial beam, efficiently sustaining the hand’s weight across a broad range of motion during various tasks. Still, this device is a semi-active device and has critical joints.

Compensating the weight of the hand is challenging as the load vector on the hand changes with the position of the hand. Thus, a constant torque must be provided at the wrist to balance the hand for DMD patients. Developing the Constant-Torque-Compliant mechanism (CTCM) for wrist exoskeletons is a novel method and presents a valuable contribution as there are very limited applications. This compliant mechanism, CTCM, is particularly valuable in applications requiring a stable output torque regardless of variations in the input rotation angle within a desired range of motion. Hou et al.[16] introduced a functional joint as a compliant CTCM, demonstrating its potential in various applications. Prakashah et al.[22] employed variable-width spline curves followed by topology optimization to synthesize a compliant CTCM, offering flexibility and adaptability in achieving constant torque output. Additionally, Phan et al.[28] developed a Compliant Torque Mechanism (CTM) suitable for rehabilitation devices such as knee joints using shape optimization, expanding the potential applications of compliant mechanisms. However, one of the major drawbacks observed in these CTCMs is that the range of constant torque those mechanisms provide is quite less (working range of $40^\circ - 60^\circ$). Therefore, such mechanisms are not suitable for the wrist support application.

This paper aims to develop a wrist exoskeleton with a constant torque-compliant mechanism that caters to the wrist’s specific range of motion requirements. This novel approach focuses on developing a compliant mechanism model that provides constant torque by optimizing design parameters. By leveraging this innovative design methodology, we intend to create a full-scaled prototypical exoskeleton dedicated to wrist support applications. By implementing this proposed design method, we aim to overcome the limitations observed in existing constant torque-compliant mechanisms and wrist supports.

This paper first discusses the design synthesis for the gravity balancer of the wrist exoskeleton. This section focuses on understanding wrist kinematics and dynamics. It employs a method to generate conceptual models followed by an optimization technique to develop a model that gives constant torque deflection. Later in the section, the model generation is presented. The work’s second part emphasizes the Constant Torque Compliant mechanism (CTCM) plots of the optimized model and its comparison of the torque deflection plots in achieving the desired constant torque output. Simulations and experiments are conducted to validate the effectiveness of the CTCM design. These outcomes provide concrete evidence of the feasibility and practicality of the final integrated design, showcasing its ability to deliver consistent and reliable torque performance. Finally, the work culminates with a concise

discussion and conclusion that summarizes the key findings and implications of the study.

II. METHODS

In this section, we elaborate on the requirements essential for the design of the Constant-Torque-Compliant Mechanism (CTCM) from wrist dynamics. Followed by the subsequent steps that involve problem formulation, optimization, synthesis procedures, and model generation. The results and interpretations derived from this approach are further validated using experimental data obtained from the prototype model.

A. Design synthesis

1) Wrist Kinematics

The wrist joint typically exhibits three degrees of freedom, as demonstrated in Figure 1: pronation/supination, involving the rotation of the radius around the ulna in the forearm, wrist flexion/extension, and ulnar/radial deviation [26]. These hand movements play a pivotal role in changing positions and grasping objects, with the wrist serving as the crucial joint enabling multi-directional hand motions. Moreover, the wrist stabilizes the hand in specific positions by providing adequate support to facilitate these movements [29][21].

Pronation/supination and flexion/extension allow for a wide range of motion during the hand movement. However, for individuals with Duchenne muscular dystrophy (DMD), these ranges of motion are affected, as observed in a study by Palmer et al.[27]. From a case involving the Wearable Robotics integration project’s wrist support [7], it is found that in individuals with DMD, the minimum range of motion for flexion and extension is found to be 80 degrees, with a range from 55 degrees (flexion) to -25 degrees (extension). Similarly, the range of motion for pronation-supination ranges from 10 degrees to 140 degrees.

Since this paper focuses on supporting flexion and extension (gravity balancing), the range of motion for these movements is visualized and represented in Figure 2.

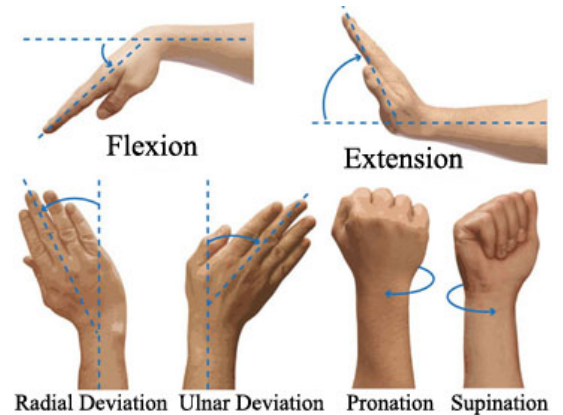


Fig. 1: Degrees of freedom of the hand [23].

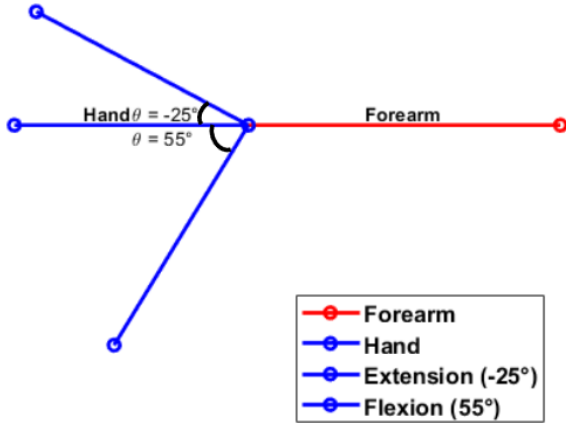


Fig. 2: Visualization of the hand's range of motion for flexion and extension with respect to the forearm.

2) Wrist Kinetics

A body exhibiting rotational motion in space possesses three degrees of freedom (DOF), which correspond to rotations about each of the three axes: yaw, pitch, and roll. Consequently, describing the motion of the hand requires three rotations to represent its degrees of freedom, with each rotation occurring around the corresponding coordinate axis.

Specific assumptions are made to define these angles associated with the motion of the hand [Figure 1](#), [Figure 2](#). The angle representing the hand's flexion and extension is θ , while the angle representing pronation and supination is ψ . Finally, the forearm flexion and extension angle is represented as ϕ . All three angles are utilized to express the energy associated with the hand's motion.

It is essential to note that these angles only possess physical significance in scenarios where the degrees of freedom of the shoulder are disregarded. Nonetheless, the potential energy of the hand, utilizing the aforementioned angles, can be expressed as [Equation 1](#) [37] [4].

$$V = m \cdot g \cdot L \cdot \sin(\theta + \phi) \cdot \cos(\psi) \quad (1)$$

Since support is being provided for the patients bound to the wheelchairs, the angle made by the forearm flexion and extension is assumed to be 0° . Moreover, the system has been specifically designed to support a single degree of freedom: flexion and extension. Considering these conditions, [Equation 1](#) the system's potential energy can be expressed as [Equation 2](#).

$$V = m \cdot g \cdot L \cdot \sin(\theta) \quad (2)$$

Using the flexion/extension angle (θ) and potential energy from [Equation 2](#), the torque exerted at the wrist due to the

gravitational force acting on the hand can be formulated as [Equation 3](#).

$$T = m \cdot g \cdot L \cdot \cos(\theta) \quad (3)$$

From [Equation 3](#), it can be observed that the motion of the hand is similar to a simple pendulum but with a different reference axis. Considering the mass of the hand (m) to be 0.4 kg [36] and assuming the length of the hand's center of gravity from the wrist joint (L) to be 95mm, the torque-deflection plot for the hand is represented in [Figure 3](#).

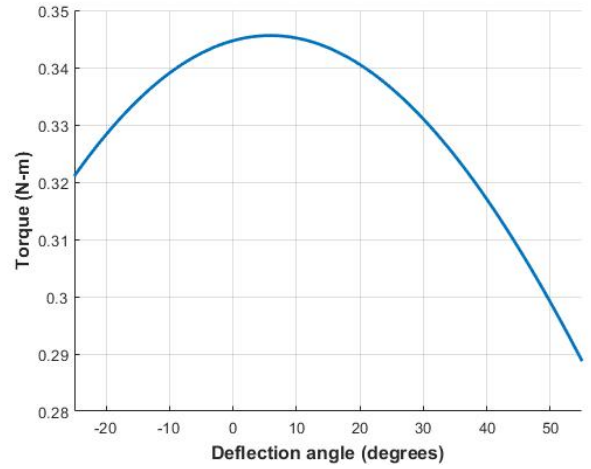


Fig. 3: Torque deflection plot for the wrist joint for -25° extension and 55° flexion.

From the kinetics of the wrist for flexion/extension [Figure 3](#) and considering the fact that muscles in hand have certain stiffness [10],[8], the required plot has been simplified to achieving constant torque profile of 0.32 N-m, and it serves as the reference for evaluating the error between the desired output and the actual performance of the analytical model [28]. The plot depicted in [Figure 4](#) illustrates the torque output of the compliant mechanism as it undergoes deflection, considering the structural characteristics and material properties incorporated in the model.

3) Concept Generation

To create a compliant mechanism, a traditional rigid body mechanism has been developed i.e. capable of providing the desired motion. The analysis focuses on a single branch comprising five slender links [16]. The mechanism consists of 5 links and 6 joints, with the first link pivoted at joint 1 and the last link pivoted at joint 6. After setting these conditions to the mechanism and inputting the rotation angle at the first joint, the mechanism produces the required motion but not the desired range of motion. Through this process, we discovered that achieving the desired range of motion requires different orientations of the mechanism or a new mechanism with additional joints and links.

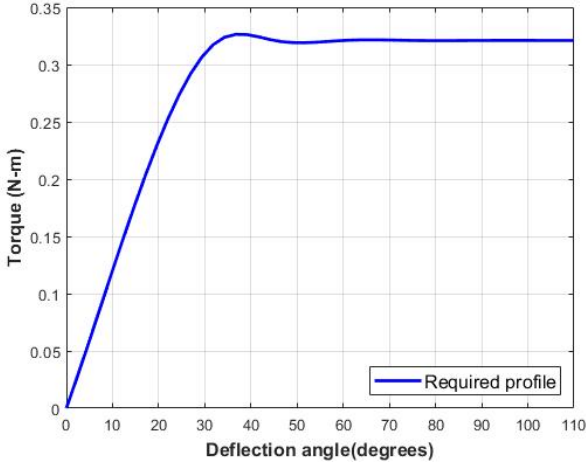


Fig. 4: The required torque deflection plot that represents the simplified torque profile that needs to be achieved by the compliant mechanism across a range of deflection angles[28]

Any number of additional links/elements can be added to the model, depending on the requirement. However, this may sometimes introduce singularity, which can, in turn, affect the degrees of freedom and range of motion. To prevent such conditions in the mechanism, it is transformed into a parametric beam structure, allowing adjustments in the positions of its points. The structure is assumed to possess specific characteristics, such as elastic deformation in response to inputs and symmetry about the center of rotation. Leveraging these assumed attributes, the mechanism's structure is modified accordingly. The joints are treated as nodes in this derived kinematic mechanism, while the connecting lines are viewed as elements. The design variables, namely the radius of the compliant mechanism (r mm) and the angle between the line joining the node and horizontal axis (P degrees) Figure 5, enable the structural modification of the mechanism through discretization of the control points (Equation 4 and Equation 5) within predefined ranges ($r = [0, 30]$, $P = [0, \pi]$).

As mentioned earlier, adding more joints (nodes/control points) impacts the mechanism's degrees of freedom and range of motion. Therefore, the number of control points becomes a crucial input during model generation.

$$x_i(r, P) = r \cos(P) \quad (4)$$

$$y_i(r, P) = r \sin(P) \quad (5)$$

So, these control points ($f_i = (x_i, y_i)$) are used to define the geometry of the system. These coordinates are defined on a 2-D plane (X-Y axis). The generated structure is a beam element model with a discrete shape. Thus the beam shape is parameterized using the B-splines, where the control points (C_i) define the beam's shape. A fourth-order B-spline is used to interpolate the spline shape. In the B-spline, a knot vector

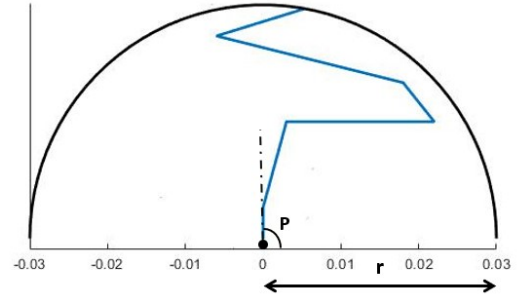


Fig. 5: One random beam element model formed from design variables showing the discrete shape of the flexure before introducing the B-splines.

has been used to make sure that the first and the last control point of the beam are clamped to the start and end points of the beam itself [24]. This method removes the discontinuity when there is a sudden dimensional change in the structure and produces a smooth transition curve with optimized parameters and a continuous beam. The surface obtained from the smooth transitioned curve is further discretized, and the number of discretization steps depends on the resolution of the beam. An increase in the number of steps increases the resolution of the beam. Thus, the optimal results can be obtained Figure 6.

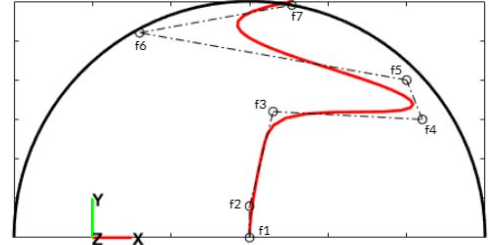


Fig. 6: The 2-D smooth transitioned curve obtained after using B-splines to the discrete shaped model and control points derived from a set of design variables are depicted.

B. Optimization

A defined objective function is utilized in conjunction with appropriate boundary conditions to obtain optimal results. A geometrically nonlinear solver that accounts for the non-linearity resulting from large displacements and rotations is employed [24]. The optimal solution is achieved by minimizing the error associated with the objective function. This optimization process aims to find the values of the design variables, leading to the best possible outcome according to the set objective Equation 10.

1) Problem statement formulation

A specific set of boundary conditions are established to constrain the model, as illustrated in Figure 7. To obtain

the model, the cross-section of the curve is defined with uniform width and height. Each node's degrees of freedom within the model is denoted by V . The first node, where the input is provided, is labeled as V_1 , and the corresponding boundary conditions are specified accordingly. Conversely, the last node in the model is treated as a fixed constraint, denoted by V_2 , and its respective boundary conditions are defined. These boundary conditions are represented by Equation 6, Equation 7 (θ_i is the input angle that is equal to the range of motion at the wrist), and Equation 8, ensuring that the model is appropriately constrained and operates within the desired parameters. The defined constraints at V_1 and V_2 play a crucial role in the behaviour and stability of the system, influencing the final results obtained through the geometrically nonlinear co-rotational beam elements solver.

$$V = [X \quad Y \quad Z \quad R_X \quad R_Y \quad R_Z] \quad (6)$$

$$V_1 = [0 \quad 0 \quad 0 \quad 0 \quad 0 \quad \theta_i] \quad (7)$$

$$V_2 = [0 \quad 0 \quad 0 \quad 0 \quad 0 \quad 0] \quad (8)$$

2) Optimization of CTCM

Finding the flexure design that delivers a constant torque output profile involves generating a constant torque profile as a crucial step. The simplified constant torque profile Figure 4 serves as an objective for the design process. By generating the constant torque output profile (T_r), the design exploration is guided toward achieving the desired torque behaviour from the flexure (T_g). This constant torque boundary condition plays a pivotal role in determining the flexure's optimal design parameters and geometry to ensure that it consistently produces the required torque output across its range of motion or operational conditions.

The main objective of this system is to minimize the discrepancy between the required constant torque profile and the constant torque profile generated by the random model, regardless of the input angle of rotation, range of motion of hand -25° to 55° Equation 10. The optimization formulation is depicted in Table I.

$$F_{obj} = \min(E) \quad (9)$$

The simulations are employed to model with a geometrically nonlinear co-rotational beam elements solver based on the Euler beam theory [3], [5]. The error (e_j) is computed as the normalized root mean square error between the required torque profile (T_r) and the torque profile (T_{gj}) generated by one of the models using a specific set of control points. The error measurements are conducted for multiple models to determine the values of e_j . These errors are then organized into an Error matrix (E), representing the subset of all the standard errors obtained from all the models (j number models).

$$e_j = \sqrt{\frac{\sum (T_{gj} - T_r)^2}{n}}, n = (\theta_2 - \theta_1) \quad (10)$$

$$E = [e_1 \quad e_2 \quad e_3 \quad \dots \quad e_{j-1} \quad e_j] \quad (11)$$

The model that exhibits the low error value can be identified by analyzing the Error matrix (error should be less than 5%). This selection process ensures that the model chosen exhibits the closest match to the required constant torque profile, making it the optimal design for flexure in the constant torque-compliant mechanism, allowing for constant torque output across the entire working range (-25° to 55°).

3) Model generation

The analysis and optimization process initially concentrated on a single flexure to achieve a constant torque-compliant mechanism. However, the analytical results presented in Figure Figure 11 indicated that the torque profile's magnitude (T) in the single flexure model had successfully attained the desired torque. The design was modified to enhance the mechanism's reliability and create a fail-safe design. This involved converting the single flexure Equation 12 into three flexures, each governed by equations (Equation 13), (Equation 14), and (Equation 15), and subsequently connecting them in parallel within the compliant mechanism, as depicted in Figure Figure 7b. This approach was adopted to address practical challenges encountered during the integration and operation of the mechanism in the device, effectively simplifying the implementation process. The resulting torque of the three-flexure model is formulated in Equation 16

$$T_{net} = T \quad (12)$$

$$T_1 = k_1 \cdot \theta_1 \quad (13)$$

$$T_2 = k_2 \cdot \theta_2 \quad (14)$$

$$T_3 = k_3 \cdot \theta_3 \quad (15)$$

$$T_{net} = T_1 + T_2 + T_3 \quad (16)$$

Where θ_1, θ_2 , and θ_3 represent the deflection angles, while k_1, k_2 , and k_3 symbolize the stiffness associated with each of the three flexure elements. To make the flexures design symmetric, each flexure is defined to have the same stiffness ($k_1 = k_2 = k_3$). Since the flexures are assumed to be connected in parallel $\theta_1 = \theta_2 = \theta_3$, thus, the combined effect of all three flexure elements (T_{net}) consequently results in the desired net torque (T).

$$T_{net} = 3 * T_1 \quad (17)$$

$$(18)$$

Objective:Finding the model with minimal torque variation using [Equation 11](#)

Design Variables:Control points: $C_i(f_i, f_{i+1})$, ($i=1$ to 6)

Constraints:

Boundary conditions:

$$g_1 : V_1$$

$$g_2 : V_2$$

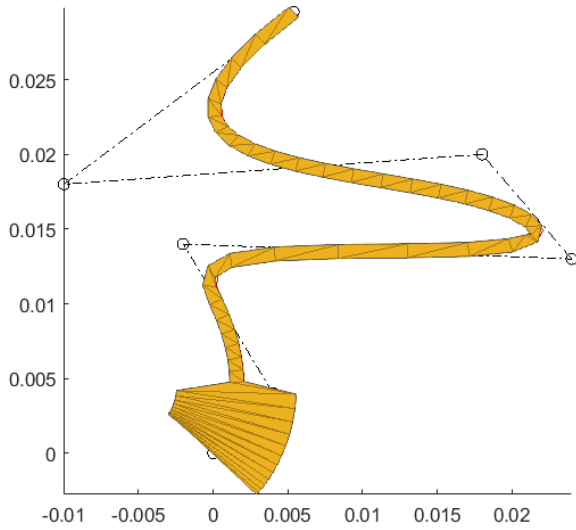
$$\text{The maximum stress, } g_3 : \sigma = \frac{\sigma_y}{SF}$$

Set constraints:

$$g_4 : r \leq 0.30$$

$$g_5 : 0 \leq \theta \leq 180$$

TABLE I: Optimization formulation of the Constant torque compliant mechanism



(a) Single flexure of the optimized model with the control points



(b) Complete model of the joint with all the three flexures

Fig. 7: Optimized model of the Constant torque compliant mechanism

Using multiple flexures in parallel not only makes the mechanism redundant but also makes it more suitable for wrist exoskeleton practical applications.

Moreover, the moment caused by the weight of the hand is effectively balanced by transferring the weight to the forearm. This weight transfer occurs by supporting the hand's weight at the center of gravity of the forearm, ensuring a balanced and comfortable experience for the user [Figure 8](#). By efficiently distributing the load using the braces and the optimized compliant mechanism model, the wrist exoskeleton provides necessary support and assistance during hand movements [Figure 9](#), reducing strain and fatigue on the user's wrist and hand muscles.

4) Experimental setup

The determination of torque variation with respect to deflection within the desired range of motion involves manufacturing a physical model of the optimized design using the Fused Deposition Modeling (FDM) 3D printing technique with Poly-

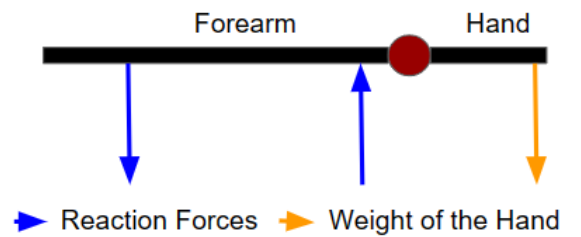
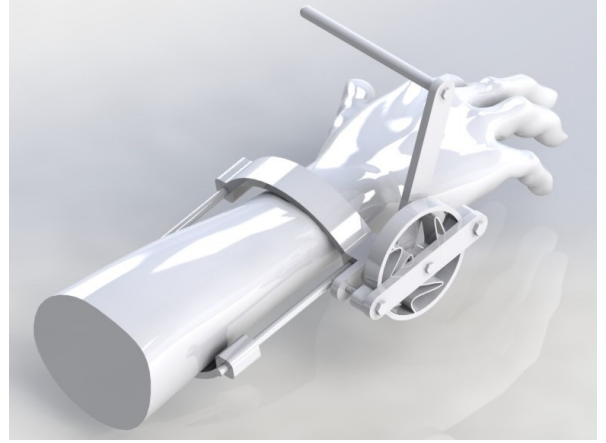


Fig. 8: Free body diagram of the setup with the braces on the hand.

lactic acid (PLA) material. This physical model aims to validate and verify the torque behaviour of the constant torque-compliant mechanism in real-world conditions. To perform the measurement of the physical model, the outer ring of the compliant mechanism is fixed. In contrast, the input torque



(a) Integration of the CTCM with the exoskeleton



(b) Assembly of the exoskeleton with the hand

Fig. 9: Wrist support exoskeleton

is applied at the center of the joint, following the boundary conditions mentioned in Equation 7 and Equation 8. A rotating torque sensor that works on the strain gauge technology is used for the measurement of the torque generated by the compliant mechanism in response to the applied deflection, as shown in Figure 10. The physical model is securely fixed to a bench vice to keep the outer ring immobilized, and the input torque is then applied manually at the other end of the test setup.

III. RESULTS

The torque profile corresponding to the deflection of the compliant mechanism is presented upon using the procedure outlined in II-A3,II-B. The following sections detail various aspects of the analysis and design process:

- 1) Plot of the Optimized Model: The optimized model, achieved by parameterizing the beam element model, having a discrete shape using a 4th-order B-spline, is plotted, demonstrating the improved design.
- 2) Comparison of Optimized and Required Plot: A comparison is made between the torque profiles of the optimized model and the required torque profile, illustrating how closely the optimized model matches the desired output.
- 3) Comparison of Optimized and discretely shaped model Plot: To understand the impact of introducing the B-splines in the model.
- 4) Mechanical behaviour with Materials: The torque profile is analyzed with respect to other materials that can be used in the development of flexure, exploring the influence of the mechanical properties of different materials on the mechanism's behaviour.
- 5) Measurement Results: A torque measurement setup is used for measuring the data, and the results obtained from the measurements are compared with the analytical results, validating the effectiveness and accuracy of the design.

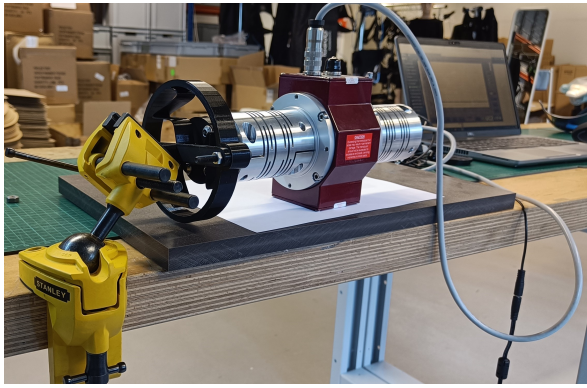
These shall comprehensively analyze and demonstrate the performance and suitability of the Compliant mechanism (CTCM) for achieving the desired constant torque output across different deflection angles. The experimental validation ensures the practical applicability of the proposed design.

A. Analytical results

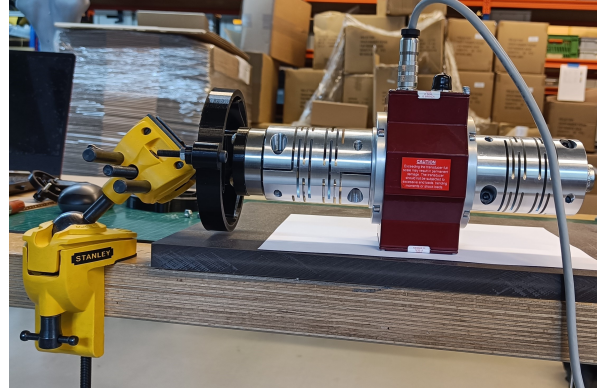
In this analysis, PLA is chosen as the CTCM material. PLA is widely recognized and well known for its various prototypical applications and is particularly popular in desktop 3D printing [32],[9], [33], [18]. Although PLA has limitations such as low strength and toughness, this is one of the best choices when flexibility is needed [30]. This modelling assumes that the material behaves linearly elastic and isotropic. This simplification allows for a more straightforward analysis and enables the use of traditional linear elastic material models.

The two key material properties used in the modelling are the modulus of elasticity and the shear modulus of the PLA material. These properties help characterize the elastic behaviour of the material and are essential for determining the flexure deflection and torque response under different loading conditions. By assuming that PLA is a linearly elastic and isotropic material, the analytical model can effectively simulate and predict the flexure's performance, ensuring that it meets the desired constant torque output requirements.

The plot in Figure 11 displays the torque profile of the optimized model, which exhibits a low error when compared with the required model. Notably, the torque profile is nearly constant for the deflection of the Compliant Torque compliant mechanism (CTCM) from 30° to 110°. The region before the constant torque, where the torque increases, is identified as the pre-stress region. This pre-stress region is considered when integrating the CTCM into the system. Considering the pre-stress region is crucial for understanding the behaviour of the CTCM and ensuring its optimal functioning. By integrating the CTCM into the system while considering the pre-stress region,



(a) Isometric view of the test setup



(b) Front view of the test setup

Fig. 10: Torque measurement setup of the sample

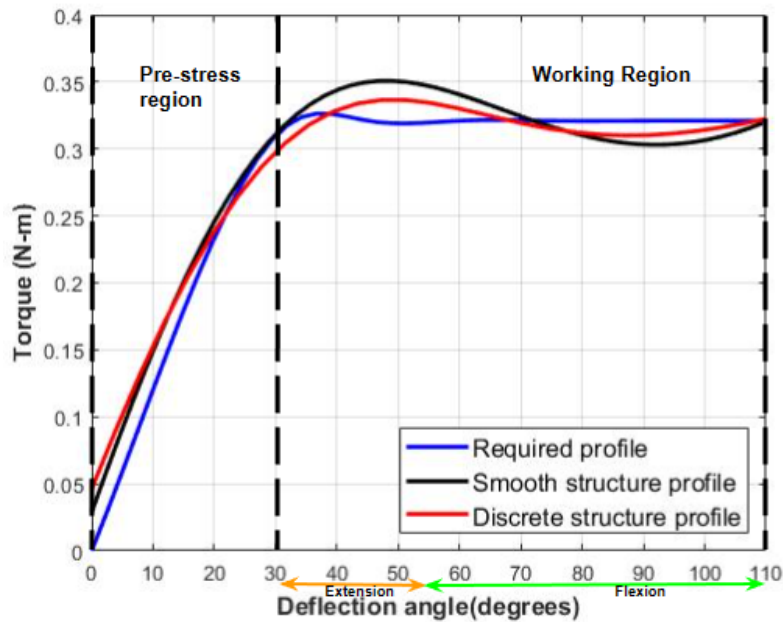


Fig. 11: Comparison of the required torque deflection plot with the discrete-shaped beam and optimized model after introducing B splines. The pre-stress region and the constant torque region, defined as the working region, are also depicted.

the overall performance of the mechanism can be effectively controlled and adjusted to achieve the desired constant torque output profile throughout the working range of the CTCM.

Additionally, in Figure 11, a comparison plot illustrates the torque profile of the generated model that yields a low error when compared with the required output torque profile. This comparison serves as validation, confirming that the optimized model effectively matches the desired constant torque output profile. Both plots provide valuable insights into the performance of the compliant mechanism and its ability to generate the required torque profile, ensuring its efficacy and accuracy for the intended application.

Besides comparing the required and optimized plot, the beam

element model before introducing the B-splines has been compared with the optimized model with a continuous structure with smoothly transitioned curvature. The plot in Figure 11 compares the torque profiles of the two models with the required profile.

The comparison of torque profiles allows us to assess the impact of introducing the B-spline parameterization on the behaviour of the compliant mechanism. The plot reveals how the discrete-shaped structure contributes to torque variations, particularly at the connection points between the flexures. On the other hand, the optimized model, with its smoothly transitioned curvature, demonstrates a more consistent and stable torque output throughout the deflection range. The optimized

model's torque profile showcases its ability to maintain a constant torque output, meeting the desired requirements and outperforming the discrete-shaped model.

After achieving the final optimized model, a comprehensive study was conducted to investigate the effect of deflection on the torque profile for the same model but with different materials, as depicted in Figure 12. This exploration aimed to understand how different materials impact the constant torque profile. During this systematic analysis, a significant realization emerged that the torque profile is not solely influenced by the material properties (E) but also by the cross-section of the flexure, which is a geometrical property (I) that affects the material's stiffness Equation 19.

$$M = \frac{E * I}{R} \quad (19)$$

From Equation 19, it has been observed that achieving a constant torque profile of the same magnitude can be accomplished for any material by appropriately adjusting the cross-section of the flexure in correspondence with the material's Young's modulus. In Figure 12, the plot shows the torque profiles of the existing optimized model with different materials. Thus, this analysis highlights that selecting appropriate materials with suitable cross sections (for PLA, it is $10*0.7$, and for titanium, it is $10*0.23$) for the flexure can effectively generate a constant torque output throughout its working range, meeting the desired performance specifications for the intended application.

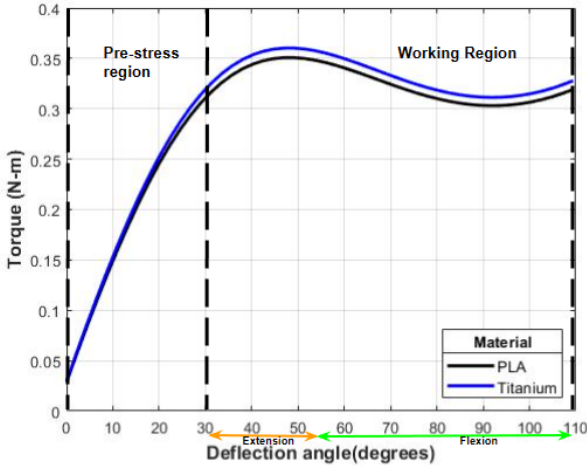


Fig. 12: Torque deflection plot for the optimized model with PLA and Titanium material.

B. Experimental results

As the deflection angle is incrementally changed within the desired range of motion, the corresponding torque values are measured using the torque measurement setup and recording the data for multiple tests. The collected data is analyzed

to determine the torque variation with respect to the deflection. This analysis allows for a direct comparison between the experimental measurements and the predictions from the analytical model. Thus, multiple tests are conducted for the prototype model to check the effect of plastic deformation. The accuracy and effectiveness of the optimized design are verified by comparing the experimental torque-deflection data with the analytical model's predictions. Any discrepancies between the experimental and analytical results are carefully examined to identify potential areas for improvement and discussed further in the section IV. The following plot in Figure 13 compares the analytical results with the measurement results from two tests.

The physical model and experimental setup provide valuable insights into the compliant mechanism's real-world behaviour, ensuring that the design meets the desired performance requirements and delivers the constant torque output within the specified working range of the CTCM.

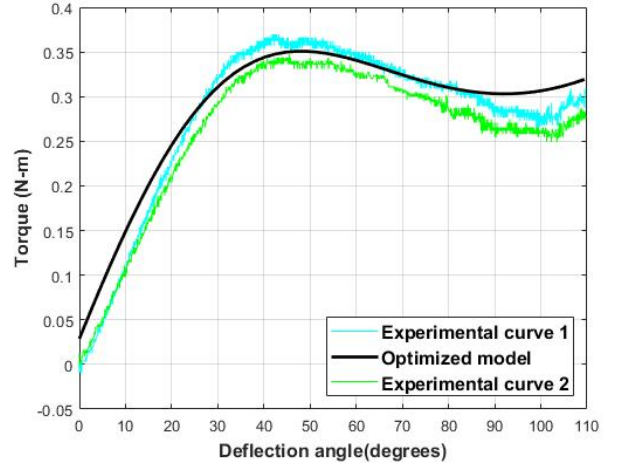


Fig. 13: Comparison of the analytical torque profile with the measured results of the sample for validation

IV. DISCUSSION

A new design approach and a parametric beam structure have been proposed. A prototypical physical model has been developed to do the experiments and validate the results. The final model is integrated into the exoskeleton and used a spring for balancing.

A. Design generation method

As mentioned earlier, the proposed design method employs an optimization approach to generate a model with the low error in torque-deflection comparison when compared to the required torque profile. However, it is important to acknowledge that the generated models within the specified bounds for the design variables may not encompass the full range of mechanical behaviours and design variations that can influence the CTCM's structure.

Due to the constraints of simulation and computational complications, exploring all possible models within the design variable space may not be feasible. The number of models generated is provided as input and evaluated with the objective function. Still, this limited sampling may not guarantee a model with a zero objective score that perfectly matches the required torque profile. To balance computational efficiency and optimization accuracy, the method prioritizes identifying a model that yields the lowest possible error (less than 5%) in torque-deflection comparison. Given the available constraints, this model is considered a good approximation of the optimal solution. It is essential to recognize that achieving a zero error between the required and optimized torque profiles may not always be realistic, especially considering the complexity of the design space and the number of possible combinations of design variables. However, by selecting a model with a low error, the proposed method ensures that the resulting CTCM design closely approximates the desired constant torque profile. Further research and advancements in computational capabilities may provide opportunities to explore a broader range of models and improve the optimization process in the future.

B. Design validation

The proposed Constant-Torque-Compliant mechanism (CTCM) design was validated using a torque measurement sensor, as depicted in Figure 10, with the corresponding boundary conditions applied. The experimental results were then compared with the torque profile plot obtained from the optimized model. The comparison revealed a small error between the experimental and analytical results, which is typical in experimental validations. Such errors can arise from various factors during the experimental setup and testing process. One potential source of error is the manual application of torque input during the experiments. The consistency of applying the load varies with time, introducing noise in the data and leading to slight discrepancies in the results. Additionally, the assumption of the material being isotropic in the design does not perfectly reflect real-world material behaviour. In reality, materials may not be perfectly homogeneous and isotropic, which can affect the overall performance of the mechanism.

Furthermore, applying boundary conditions during the experiments, such as fixing the outer ring in the model, can also influence the results to some extent. Small variations in how boundary conditions are imposed can lead to minor discrepancies between experimental and analytical outcomes. However, despite these inherent uncertainties, it is essential to consider the overall effectiveness of the proposed CTCM design. Despite the small errors observed, the torque-deflection profile of the proposed model closely aligns with the experimental results. This close match between the analytical and experimental results validates the efficacy of the CTCM design in achieving a constant torque profile over the desired range of motion. While it is crucial to acknowledge and address

any discrepancies in the experimental validation, it is equally important to focus on the overall success of the proposed design. The fact that the optimized model closely resembles the experimental results confirms the potential of the CTCM in assisting individuals with muscular disorders.

C. Future work

While the proposed design of the Constant-Torque-Compliant mechanism (CTCM) shows promising results, there are indeed some limitations and opportunities for future improvements that can be considered. Addressing these limitations will enhance the usability and effectiveness of the mechanism in assisting individuals with muscular disorders. Firstly, the current model is primarily focused on gravity balancing. Future improvements could incorporate additional features that enable the CTCM to carry some weight, thereby assisting patients in performing daily activities that involve lifting or holding objects.

Secondly, the current design assumes a fixed angle of pronation and supination at 0° . However, the wrist often exhibits some degree of pronation during flexion. To improve the accuracy and realism of the CTCM, future iterations of the design should account for the supination angle during flexion. This consideration would lead to a more comprehensive and realistic representation of the wrist's motion, enhancing the overall functionality and usability of the exoskeleton.

Third, while experimental testing and validation have been conducted, it is essential to conduct further testing with actual patients. Real-world testing would provide valuable insights into the constraints and limitations of hand motion imposed by the exoskeleton. This could also help understand how the CTCM interacts with the user's hand. Moreover, conducting patient trials would help gather feedback directly from the users, informing iterative improvements and leading to a more user-centric and effective design.

V. CONCLUSION

In conclusion, this study presents the design, optimization, and validation of a compliant mechanism (CTCM) for achieving a constant torque output within a desired range of motion for the gravity balancing of the hand. The flexure design was fine-tuned through random model development and optimization techniques to meet the specified torque requirements. The parametric optimization process involved the flexures with smooth and continuous curvature, resulting in an improved torque profile that generates an optimal for the desired range of motion (-25° to 55°).

Experimental validation of the optimized model was conducted using a physical prototype manufactured via FDM 3D printing with PLA material. The torque variation with deflection was measured and compared with the analytical predictions. The experimental results demonstrated are comparable with the analytical model, validating the optimized design's accuracy and effectiveness in generating the desired constant torque output.

Moreover, the investigation into the effect of stiffness on torque magnitude revealed the critical role of material selection and cross-section of the geometry. By changing the material properties and the cross-section of the flexure, the stiffness of the flexure could be tailored to match the required torque magnitude.

The proposed device with the CTCM proves to be robust and one of the possible solutions for achieving constant torque output, showcasing its potential applicability in supporting the wrist joint for flexion and extension as a rehabilitation device. Thus, the developed compliant model is used in the wrist exoskeleton. This research provides valuable insights for designing efficient and optimized compliant mechanisms for torque-sensitive applications.

REFERENCES

- [1] Ambrose. *Ambroise Dynamic wrist orthosis*. <https://www.ambroise.nl/en/arm-orthoses/wrist-orthoses/ambroise-dynamic-wrist-orthosis/>. 2022, June 20.
- [2] Ali Amoozandeh Nobaveh, Giuseppe Radaelli, and Just L Herder. “A design tool for passive wrist support”. In: *Wearable Robotics: Challenges and Trends: Proceedings of the 5th International Symposium on Wearable Robotics, WeRob2020, and of WearRAcon Europe 2020, October 13–16, 2020*. Springer. 2022, pp. 13–17.
- [3] Ali Amoozandeh Nobaveh, Giuseppe Radaelli, and Just L Herder. “Asymmetric spatial beams with symmetric kinetostatic behaviour”. In: *Symposium on robot design, dynamics and control*. Springer. 2020, pp. 247–254.
- [4] B.J.vanderBurgh. *Constant torque gravity compensation*. <http://resolver.tudelft.nl/uuid:cd089772-150a-49ab-833c-681e9c368dd3>. 2022.
- [5] Jean-Marc Battini. “Co-rotational beam elements in instability problems”. PhD thesis. KTH, 2002.
- [6] Luis F Cardoso, rgio Toma zio, and Just L Herder. “Conceptual design of a passive arm orthosis”. In: *International Design Engineering Technical Conferences and Computers and Information in Engineering Conference*. Vol. 36533. American Society of Mechanical Engineers. 2002, pp. 747–756.
- [7] Case involving the Wearable Robotics integration project’s wrist support. *Wearable Robotics*. <https://https://www.wearablerobotics.nl/>.
- [8] Ashlee Cruz et al. “Mobile arm supports in Duchenne muscular dystrophy: a pilot study of user experience and outcomes”. In: *Disability and Rehabilitation: Assistive Technology* 16.8 (2021), pp. 880–889.
- [9] Vincent DeStefano, Salaar Khan, and Alonzo Tabada. “Applications of PLA in modern medicine”. In: *Engineered Regeneration* 1 (2020), pp. 76–87.
- [10] Dongsheng Duan et al. “Duchenne muscular dystrophy”. In: *Nature Reviews Disease Primers* 7.1 (2021), p. 13.
- [11] Dynasplint. *Hand amp, fingers*. <https://dynasplint.com/product/hand-fingers/>.
- [12] Alan EH Emery. “Population frequencies of inherited neuromuscular diseases—a world survey”. In: *Neuromuscular disorders* 1.1 (1991), pp. 19–29.
- [13] Peter Walker Ferguson, Yang Shen, and Jacob Rosen. “Hand exoskeleton systems—Overview”. In: *Wearable Robotics* (2020), pp. 149–175.
- [14] RARC Gopura, Kazuo Kiguchi, and DSV Bandara. “A brief review on upper extremity robotic exoskeleton systems”. In: *2011 6th international Conference on Industrial and Information Systems*. IEEE. 2011, pp. 346–351.
- [15] Yasuhisa Hasegawa, Satoshi Shimada, and Kiyoshi Eguchi. “Development of wrist support mechanism for muscle weakness person to work on desk work”. In: *2014 International Symposium on Micro-NanoMechatronics and Human Science (MHS)*. IEEE. 2014, pp. 1–3.
- [16] Chia-Wen Hou and Chao-Chieh Lan. “Functional joint mechanisms with constant-torque outputs”. In: *Mechanism and Machine Theory* 62 (2013), pp. 166–181.
- [17] Laevo Flex. *Laevo Exoskeletons*. <https://www.laevo-exoskeletons.com/flex>. 2022.
- [18] Daniel Lateş, Marius Căşvean, and Sorina Moica. “Fabrication methods of compliant mechanisms”. In: *Procedia Engineering* 181 (2017), pp. 221–225.
- [19] Rajesh Luharuka and Peter J Hesketh. “Design of fully compliant, in-plane rotary, bistable micromechanisms for MEMS applications”. In: *Sensors and Actuators A: Physical* 134.1 (2007), pp. 231–238.
- [20] John Roy McGuire. *Analysis and design of constant-torque springs used in aerospace applications*. The University of Texas at Austin, 1994.
- [21] Maheen Nadeem et al. “Ulnar extension coupling in functional wrist kinematics during hand activities of daily living”. In: *The Journal of Hand Surgery* 47.2 (2022), 187–e1.
- [22] Hari Nair Prakashah and Hong Zhou. “Synthesis of constant torque compliant mechanisms”. In: *Journal of Mechanisms and Robotics* 8.6 (2016), p. 064503.
- [23] Negin Nikafrooz, Mohammad J Mahjoob, and Mohammad Ali Tofigh. “Design, Modeling, and Fabrication of a 3-DOF Wrist Rehabilitation Robot”. In: *2018 6th RSI International Conference on Robotics and Mechatronics (IcRoM)*. IEEE. 2018, pp. 34–39.
- [24] Ali Amoozandeh Nobaveh and Brandon Caasenbrood. “Design Feasibility of an Energy-Efficient Wrist Flexion-Extension Exoskeleton using Compliant Beams and Soft Actuators”. In: *2022 International Conference on Rehabilitation Robotics (ICORR)*. IEEE. 2022, pp. 1–6.
- [25] Marcos B Oliveira et al. “Design of a variable stiffness wrist brace with an origami structural element”. In: *Smart Materials, Adaptive Structures and Intelligent*

Systems. Vol. 51951. American Society of Mechanical Engineers. 2018, V002T08A009.

- [26] Nurdos Omarkulov et al. “Preliminary mechanical design of NU-Wrist: A 3-DOF self-aligning Wrist rehabilitation robot”. In: (2016), pp. 962–967.
- [27] Andrew K Palmer et al. “Functional wrist motion: a biomechanical study.” In: *The Journal of hand surgery* 10.1 (1985), pp. 39–46.
- [28] Thanh-Vu Phan, Huy-Tuan Pham, and Cong-Nam Truong. “Design and analysis of a compliant constant-torque mechanism for rehabilitation devices”. In: *Advanced Materials: Proceedings of the International Conference on “Physics and Mechanics of New Materials and Their Applications”, PHENMA 2019*. Springer. 2020, pp. 541–549.
- [29] MJ Rainbow et al. “Functional kinematics of the wrist”. In: *Journal of Hand Surgery (European Volume)* 41.1 (2016), pp. 7–21.
- [30] RSS. *What is the most flexible 3D printing material*. <https://www.3dprintingspot.com/post/flexible-material>. 2021.
- [31] L Saggere, Sridhar Kota, and SB Crary. “A new design for suspension of linear microactuators”. In: *ASME Journal of Dynamic Systems and Control* 55.2 (1994), pp. 671–675.
- [32] P Saini, M Arora, and MNV Ravi Kumar. “Poly (lactic acid) blends in biomedical applications”. In: *Advanced drug delivery reviews* 107 (2016), pp. 47–59.
- [33] Jainil Shaha, Jenish Sonia, and Pratik Moradiyab. “A Review of Compliant Mechanisms Manufactured by using 3D Printing Technology”. In: (2022).
- [34] Elliot Thompson-Bean, Oliver Steiner, and Andrew McDaid. “A soft robotic exoskeleton utilizing granular jamming”. In: *2015 IEEE International Conference On Advanced Intelligent Mechatronics (AIM)*. IEEE. 2015, pp. 165–170.
- [35] Lucas Tiziani et al. “Empirical characterization of modular variable stiffness inflatable structures for supernumerary grasp-assist devices”. In: *The International Journal of Robotics Research* 36.13-14 (2017), pp. 1391–1413.
- [36] What Things Weigh. *Weight of a hand, What Things Weigh*. <https://whatthingsweigh.com/how-much-does-a-hand-weigh/>. 2021.
- [37] Volkert van der Wijk and Just L Herder. “Synthesis of dynamically balanced mechanisms by using counter-rotary counter mass balanced double pendula”. In: (2009).
- [38] Li Zhang et al. “Assistive devices of human knee joint: A review”. In: *Robotics and Autonomous Systems* 125 (2020), p. 103394.

4

Conclusion

4.1. Contribution

This research introduces a novel compliant mechanism designed to achieve gravity balancing of the wrist during flexion and extension movements. Unlike traditional wrist support approaches, incorporating a compliant mechanism within the exoskeleton framework presents several advantages, including reduced part count, minimized joint friction, and decreased energy losses.

Chapter Two of this report offers an insightful survey of mechanisms showcasing varying stiffness behaviour and those displaying constant torque and force behaviour under variable loading conditions. These mechanisms find application in diverse fields, such as aerospace, transmission, and the medical domain. The chapter delves into the mechanics of these mechanisms within specific applications, elucidating their operational principles. Classification is subsequently applied based on the underlying working principles, enhancing comprehension.

Moreover, the chapter assesses these mechanisms, considering performance parameters and prerequisites. This evaluation provides valuable insights for the subsequent stages of concept development, particularly about creating a gravity balancer for hand support. This chapter lays a solid foundation for the next chapters to delve into the intricate development and analysis of the proposed mechanisms.

In chapter three, a comprehensive understanding of wrist kinematics and kinetics is presented, along with a simplified mechanical behaviour of the wrist. A distinctive design strategy is introduced, involving manipulating design variables to change the shape of the flexure. The optimization process scrutinizes a range of designs formed from a set of design variables to pinpoint the one that best emulates the intended mechanical behaviour. The efficacy of this mechanism's mechanical behaviour is subsequently confirmed through experimental validation, facilitating a comparison with simulation outcomes.

Furthermore, the report presents a brace design that effectively supports and redistributes the load from the hand to the forearm. The culmination of this chapter involves integrating the final model and the developed brace system. This holistic approach ensures the applicability of the devised mechanism within practical devices, cementing its real-world utility.

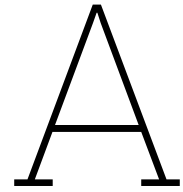
4.2. Future work

By marking a significant stride, this research lays the groundwork for further inquiries that could refine and expand upon the proposed design, thereby contributing to the advancement of assistive technologies catering to conditions like DMD. While this research presents a pioneering solution through the novel design, certain aspects remain open-ended, prompting new avenues for future investigations.

To begin with, the simplified assumption regarding the torque deflection behaviour required for the hand, predicated considering the muscle stiffness, warrants further exploration. Conducting empirical tests to elucidate the influence of muscle stiffness in the hands of individuals with DMD could provide valuable insights into refining the model.

In the existing model, the influence of impedance at the mechanism joint has been disregarded, as the primary aim is to achieve balancing the hand weight. However, the difference between the profiles can be observed in the experimental outcomes. As such, future analyses should account for joint impedance and undertake appropriate compensation.

Furthermore, the current balancing has been tailored to one of the hand's movements, yet it's pivotal to acknowledge that the hand poses the pronation/supination motion during flexion and extension. To address this, forthcoming research should delve into the potential for stiffness adjustment within the proposed mechanism, thus enhancing adaptability for both degrees of freedom.



Experimental setup

A.1. Test Protocol

A torque sensor was utilised during the experimentation process to validate the results of the developed compliant mechanism, as shown in Figure A.1 and measure the torque required to deflect the mechanism. Using this sensor, a stable and reliable test setup was developed to assess the effectiveness of the constant gravity compensation compliant mechanism through experiments. Ensuring the accuracy and validation of the experimental results required following specific precautions during the testing process, which are outlined as follows:



Figure A.1: Torque sensor

1. **Alignment of Axis:** To maintain precision and consistency, great care was taken to ensure that the axis of the torque measurement sensor and the compliant mechanism were perfectly collinear or in line. Misalignment could introduce errors in the torque measurements and result in applying the input load on unintended axes besides the intended, leading to inaccurate and misleading results.

2. **Fixing the Outer Ring:** The compliant mechanism's outer ring was securely fixed to prevent unintended movement or displacement during the experiment, which could lead to inaccurate data. This step is crucial for maintaining stability in the test setup and getting reliable data.
3. **Controlled Torque Application:** The torque was applied manually with a steady and consistent rate to ensure less disturbance in the data. This controlled torque application helps to increase the accuracy of the measured compliant mechanism's response without much disturbance in the collected data.
4. **Range of input:** The input rotation angle during the experiment was carefully monitored to ensure it fell within the required range of motion for the wrist joint (flexion/extension). Giving the rotation input angle for the specified range is essential for obtaining the relevant data.

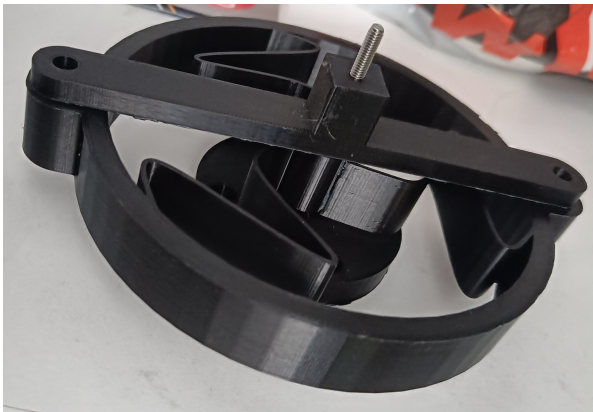
Adhering to these precautions was essential to optimize the experimental setup for accurate data collection.



(a) Fixing mechanism to the bench vice



(b) Assembly of additional support between mechanism and sensor



(c) Assembly of two points fixating to single point fixating of the mechanism



(d) The line drawn on the paper to check the alignment of the set-up is highlighted

Figure A.2: Test set up with the torque sensor

A.2. Fixing the compliant mechanism

During the test setup, the compliant mechanism's outer ring was securely fixed to a bench vice Figure A.2a, ensuring its stability and preventing any unwanted movement during the experiment. In Figure A.2c, an image of the assembly of the mechanism used for the test setup to fixate is depicted. In

this image, the two fixating mounting points typically used for fixing the outer ring of the compliant mechanism have been modified and converted into a single point for fixing. This modification has ensured that the mechanism has no out-of-plane orientation, and thus, the unintended loads can be avoided. By consolidating the two fixating points into a single fixing point, we aimed to create a reliable setup. The centre of the mechanism, where the input was provided, was connected to the torque sensor using additional support, effectively transmitting the manually applied load to the mechanism (Figure A.2b).

To ensure accurate measurements, verifying the alignment of the mechanism's axis with the torque sensor was crucial. For this purpose, a straight line was drawn on paper, representing the axis of the compliant mechanism and the torque sensor. By aligning the axis of the compliant mechanism and the torque sensor with this drawn line, it is ensured that they are collinear or in line with each other (Figure A.2d). This alignment was essential to obtain precise and reliable torque measurements throughout the experiment. Any deviation from the alignment could introduce errors in the recorded data, potentially affecting the evaluation of the compliant mechanism's performance in providing constant torque.

A.3. Input torque

Ensuring proper alignment and fixating is indeed crucial, but it alone may not be sufficient to eliminate disturbances in the data. Its small size in the developed compliant mechanism model can lead to discrepancies and variations in the data. To address this issue, the model has been scaled by a factor of 2. Scaling the model allows for more accurate and consistent measurements, reducing data distribution. When the model is scaled, certain parameters such as the cross-section, moment of inertia (I_o), and bending stiffness (M_o) are affected.

$$I_o = \frac{w \cdot h^3}{12}$$

$$M_o = E \cdot I_o$$

Where w and h represent the width and height of the original model, respectively.

Since the height and width of the model are doubled after scaling ($w_m = 2 \cdot w$, $h_m = 2 \cdot h$), the new moment of inertia (I_{new}) and stiffness (M_{new}) of the mechanism increase accordingly.

$$I_{new} = 16 \cdot I_o$$

$$M_{new} = 64 \cdot M_o$$

As a result of this scaling, the torque-deflection plot of the model exhibits an increase in magnitude by a certain factor compared to the required plot. This change in magnitude is attributed to the increase in the moment of inertia and stiffness of the mechanism due to the scaling process. This approach ensures that the experiment effectively captures the constant torque compensation capability of the compliant mechanism.

In the experimental setup, the torque is applied on the opposite end of the torque measurement sensor, as indicated by a black arrow in Figure A.3. This arrangement allows for the manual application of torque with a steady and consistent force. By applying the torque manually with the hand, the motion at the sensor's input side replicates the hand's movement, simulating the natural interaction between the wrist joint and the compliant mechanism.

During the experiment, special attention was given to monitoring the input rotation angle to ensure it fell within the required range of motion for the wrist joint. While experimenting, the torque could be increased or decreased with changes in the hand's position along the sensor during the input rotation angle, which introduced disturbance in the data. Therefore, care has been taken to provide the input without changing the hand position. However, multiple tests have been conducted to verify the data and evaluate the compliant mechanism's performance under various conditions, thus avoiding human errors. This dynamic feature of the experimental setup provided valuable data on the mechanism's behaviour and response to different torque levels and rotation angles.

A.4. Final setup

These additional images provide a clear visual representation of the setup used for the experiment, showcasing the ingenuity and attention to detail applied to ensure the test's success Figure A.3. Such meticulousness in the experimental setup is crucial in obtaining valid and meaningful data, allowing for a comprehensive evaluation of the compliant mechanism's performance in providing constant torque compensation.

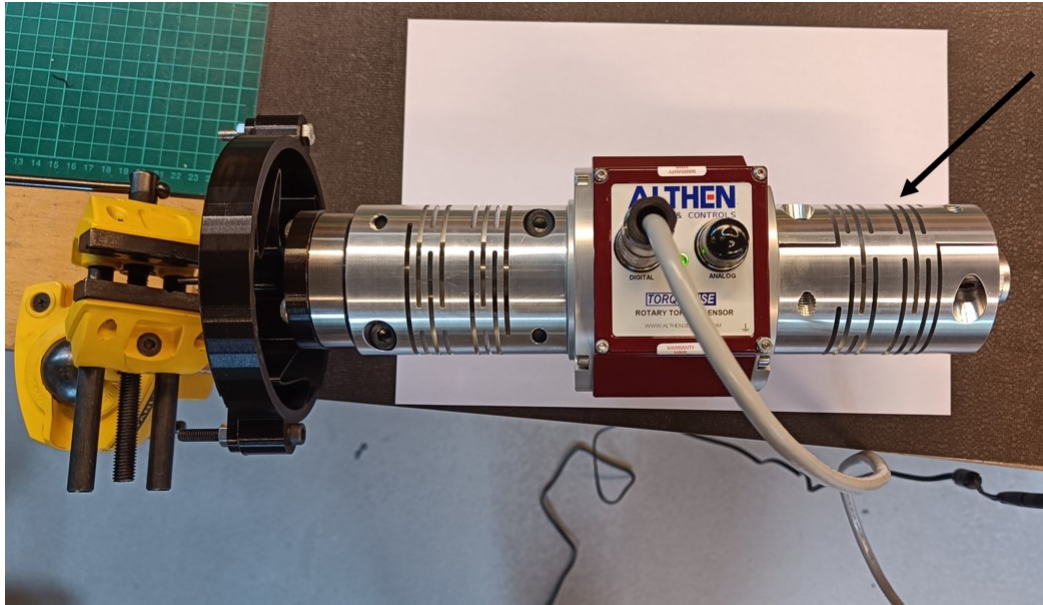


Figure A.3: Final set up of the mechanism with the sensor

B

Analysis Results

The investigation presented in chapter 3 centres around the analysis of a developed model, primarily focusing on a single flexure component. The initial or undeformed state of the system defines the node configuration, including control points. Upon applying an input rotation angle (the desired rotation angle), observable changes in node configurations within the flexure transpire, as illustrated in Figure B.1. Throughout the deformation process of the flexures, mechanical stress emerges within the structure.

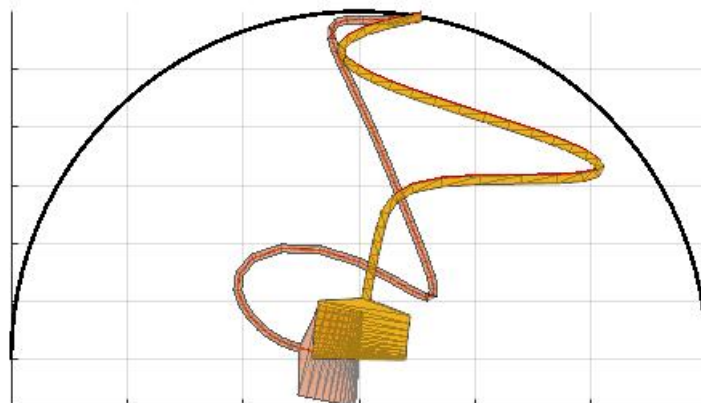


Figure B.1: The undeformed and deformed shape of the flexure in the proposed compliant mechanism chapter 3. Yellow flexure - undeformed and red flexure - deformed

B.1. Stress analysis

The stress distribution within the optimized model corresponding to the desired rotation angle is depicted in Figure Figure B.2a, and its accuracy is confirmed by comparing it with results obtained from finite element analysis (FEA).

The previously discussed line model from chapter 3 is transformed into a solid model and imported into Ansys Workbench to compare the stress results. Static structural analysis is performed within the Ansys environment using a single time step, which is preferred over multiple time steps for practical reasons.

The analysis settings are configured to employ this single-time step analysis. Complexities associated with handling the massive data generated from MATLAB simulations with numerous time steps are mitigated. The boundary conditions are applied to the mechanism such that it replicates the line model boundary conditions behaviour and simulates accurately under the given circumstances, such as fixating the mechanism and applying the optimized torque value determined from the optimization process in Matlab.

After applying these boundary conditions, a fine tetrahedral mesh is generated to ensure the fidelity of the simulation results. The simulation is then executed, yielding valuable outcomes such as the Von Mises stress distribution and strain within the mechanism.

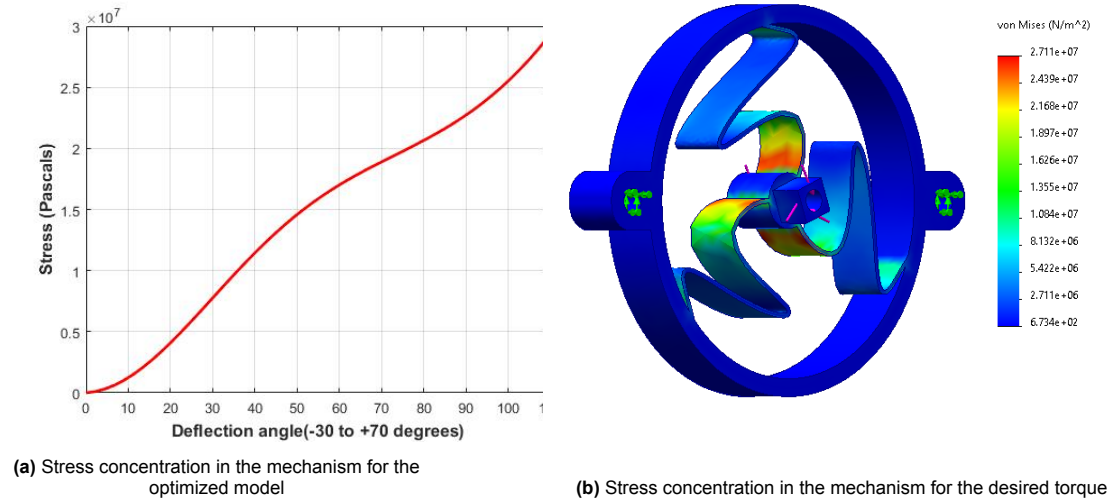
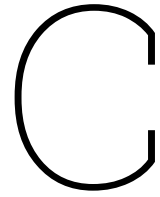


Figure B.2: Development of mechanism from curve

The validity of the stress distribution in the mechanism can be ascertained by comparing the stress results from this FEM analysis with those obtained from the optimized model in Matlab. This verification step is crucial in ensuring the reliability and accuracy of the optimized design, enabling the researchers to have confidence in the performance and structural integrity of the compliant mechanism.

The stress analysis conducted in ANSYS yielded results that closely align with those obtained from the optimized model in MATLAB, particularly when analyzing the mechanism at its maximum deflection Figure B.2b. The MATLAB analysis involves a line geometry for the flexure, while ANSYS employed a more comprehensive solid geometry for the simulation. Furthermore, the input torque applied in the MATLAB analysis closely follows the constant torque curve. In contrast, the ANSYS simulation employs a constant input torque. These variations in the analysis setup contribute to minor disparities between the results obtained from the two tools. Such concurrence between the MATLAB-optimized model and the ANSYS stress analysis instils confidence in the design's performance and validity. It indicates that the chosen parameters, boundary conditions, and optimization techniques have been successfully translated into ANSYS, allowing for a comprehensive assessment of the mechanism's structural integrity and stress distribution. This alignment further supports the robustness of the approach to developing and validating the compliant mechanism design.

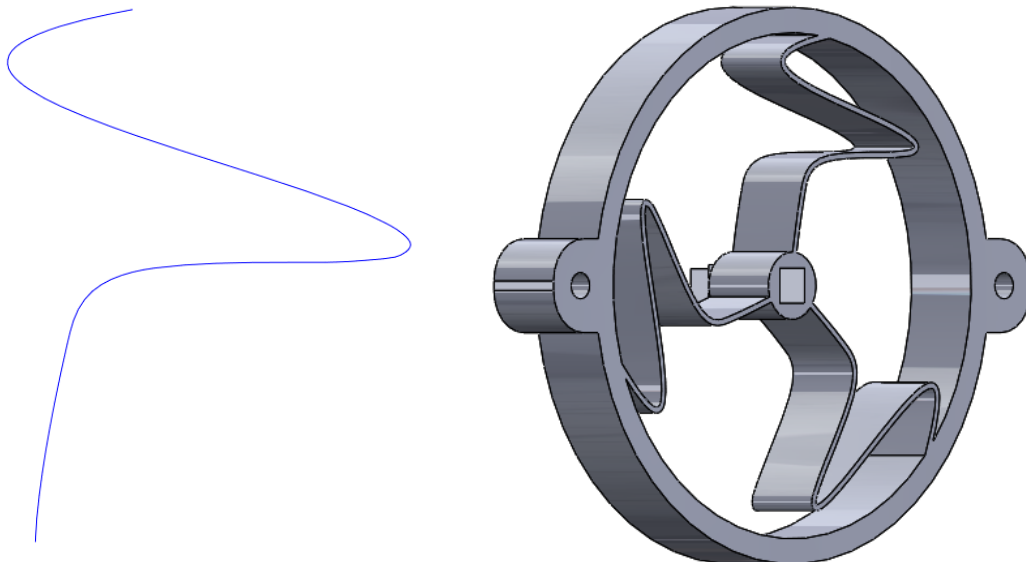


Development and Manufacturing:

To learn more about the mechanical behaviour of the developed model, a prototype of the mechanism is manufactured to perform the experiments. The CAD picture of the prototype model is Figure C.1a

C.1. Prototype development

Once the optimized curve, achieved through implementing B-splines, was obtained, the next step involved importing this curve into SolidWorks. The software-defined a cross-sectional profile along the curve, incorporating the width and thickness specifications encompassing the entire mechanism structure. This process facilitated the creation of a comprehensive 3D model that accurately represented the compliant mechanism. Subsequently, a pivotal decision revolved around selecting the most suitable manufacturing method for translating the digital model into a physical prototype. During this phase, careful consideration was given to the nodes spatial arrangement and the design's intricacies. It became evident that adhering to conventional manufacturing techniques could pose challenges due to the mechanism's complex geometry and unconventional structure.



(a) Curve obtained from the nodal points imported after simulation in matlab

(b) CAD model of the mechanism generated from the curve

Figure C.1: Development of mechanism from curve

C.2. Prototype manufacturing

The realization that conventional methods might not be feasible for manufacturing underscored the significance of exploring alternative fabrication approaches. The intricate arrangement of nodes and the unique geometry called for a method that could accurately reproduce the design without compromising its functionality. This awareness prompted the evaluation of advanced manufacturing techniques, with additive manufacturing, specifically 3D printing, emerging as a viable option for translating digital design into a physical prototype. The need for innovative approaches ultimately led to the choice of 3D printing as a suitable means of materializing the complex compliant mechanism design.

The proposed design can be produced from various manufacturing methods such as laser cutting, 3d printing, water jet cutting etc. Besides the mechanism, multiple components are required to experiment. Thus, 3d printing utilizing the Fused Deposition Modeling (FDM) technique was selected to create a scaled-up prototype of the compliant mechanism. This decision was driven by the intention to reduce manufacturing processes and avoid complexities arising from employing multiple manufacturing processes to produce various experimental setup components.

By opting for 3D printing, the challenges associated with manufacturing diversity were circumvented. Compared to traditional manufacturing, this approach offered greater flexibility in fabricating intricate parts. Acknowledging that the mechanical properties of the mechanism—like tensile strength, fatigue resistance, compression, and bending, can be influenced by 3d printing because manufacturing involves layering the material. Meticulous measures were taken to address this concern [11], specifically, employing the smallest feasible nozzle diameter, providing the dimensional tolerances for the structure, and configuring corresponding material parameters during the printing process ensured that the mechanical properties are not much affected. By adhering to these guidelines, the parts are manufactured.

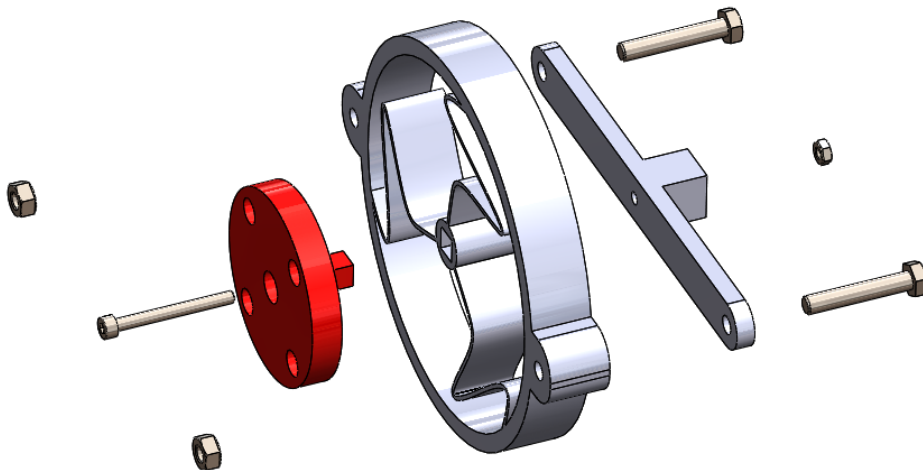


Figure C.2: Model of the parts manufactured using 3d printing FDM process

Ultimately, 3D printing, particularly in conjunction with the Fused Deposition Modeling (FDM) technique, facilitated successfully creating a prototype of the proposed compliant mechanism. This manufacturing method simplified the fabrication process and facilitated various components creation Figure C.2, paving the way for comprehensive experimental testing and validation. However, it's important to note that while the constant torque deflection curve achieved using PLA material meets the specified requirements, the mechanism does exhibit a degree of creep over multiple cycles. Nevertheless, the versatility of 3D printing helps in exploring the possibility of employing alternative materials, such as metals, to address the creep issue and potentially enhance the overall mechanical behaviour. Furthermore, the inherent flexibility of the proposed design allows for easy scaling, although this is contingent upon the available printing resolution.

D

Positive and Negative stiffness mechanism

D.1. Introduction

Achieving constant torque by combining positive and negative stiffness mechanisms is one of the promising methods. The combination of the positive and negative stiffness mechanisms results in an approximately constant torque curve, as depicted in Figure D.3. The positive stiffness mechanism provides the initial stiffness, while the negative stiffness mechanism counters the increasing stiffness and allows for a balanced torque output. This combination of mechanisms ensures continuous equilibrium, neutral stability, constant potential energy, and zero stiffness, making the combined mechanism an effective solution for gravity compensation. This section focused on initial approach of implementing this approach using a rubber spring for generating negative stiffness and a compliant mechanism for positive stiffness.

Negative stiffness is achieved through the integration of a rubber spring. The rubber spring is strategically positioned to maintain a difference in the radius of rotation between the rubber spring and the hand. As a result, when an external force is applied to the hand, the rubber spring exhibits a bi-stable nature. Simultaneously, the positive stiffness joint is created using a compliant mechanism. The combination of positive and negative stiffness components effectively cancels each other's effects, ensuring a constant torque magnitude across the desired range of motion. By changing the pre-stress in the rubber spring, the magnitude of the constant torque can be varied between positive and negative values.

The compliant mechanism allows controlled deformation during movements, providing consistent support to the wrist joint. When combined with the negative stiffness of the rubber spring, this design creates a supportive environment for the wrist muscles, enhancing the overall flexibility and comfort of the user. Implementing this approach is expected to yield several advantageous characteristics in the wrist support mechanism. These include continuous equilibrium, stability, and constant potential energy, providing a balanced and supportive environment for the wrist joint during various activities and movements.

D.2. Model

Based on the model proposed by Jensen et al. [6] on the double slider crank mechanism, a mechanism exhibits bistable behaviour when a spring is placed at either of the sliders, and the initial position is not an extreme position for the spring. Drawing inspiration from this reference model, a similar concept is applied in our design. By fixing one end of the spring and connecting the other end to the end effector (hand), we achieve a bistable nature in our compliant mechanism Figure D.1.

In this configuration, the mechanism is designed to have two stable equilibrium positions due to the difference in the radius of rotation for the hand and spring. The mechanism is unstable when the hand

is at rest or in a neutral position. However, the mechanism can transition between the two stable states when an external force or torque is applied to the hand.

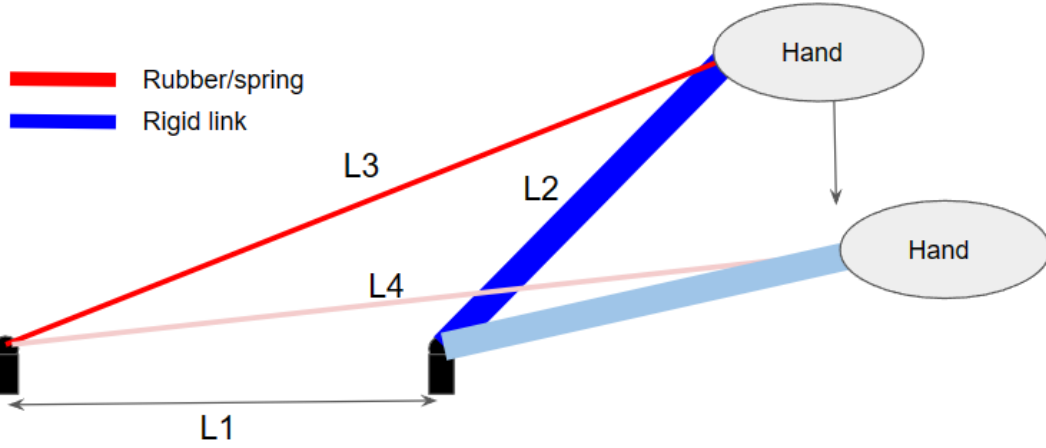
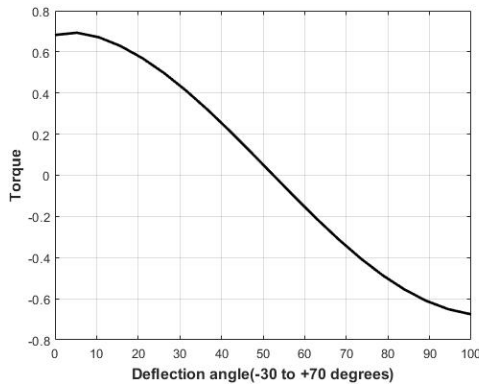


Figure D.1: Visual representation of negative stiffness mechanism showing the initial and deformed configuration

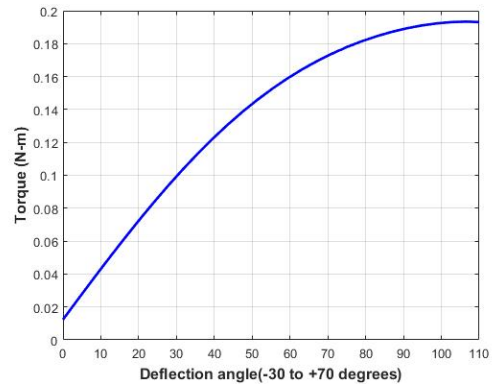
The potential energy (V) stored in the spring due to the deflection and the potential energy due to the mass of the hand can be expressed as follows:

$$V = \frac{k(l_3 - l_4)^2}{2} - m l_1 g (\cos(t) - 1)$$

$$\text{where, } l_3 = \sqrt{l_1^2 + l_2^2}, \quad l_4 = \sqrt{l_1^2 \cos(t)^2 + (l_2 + l_1 \sin(t))^2}$$



(a) Torque deflection curve of the negative stiffness mechanism



(b) Torque deflection curve of the Positive stiffness mechanism

Figure D.2: Fixating the mechanism to the torque sensor

where K is the stiffness of the rubber spring, m is the mass of the hand, l_1, l_2, l_3, l_4 are the lengths depicted in Figure D.1 and t is the angle made by the rigid link with respect to the horizontal plane. From the potential energy of the mechanism, the torque (T_r) at the wrist due to the deflection of the rigid link can be expressed as

$$T_r = k l_1 l_2 \cos(t) + g l_1 m \sin(t) - \frac{k l_1 l_2 \cos(t) \sqrt{l_1^2 + l_2^2}}{\sqrt{l_1^2 + 2 \sin(t) l_1 l_2 + l_2^2}}$$

A compliant mechanism with positive stiffness has been successfully developed by applying the parametric optimization process described in chapter 3. This mechanism exhibits a softening behaviour, meaning that the stiffness decreases as it deflects Figure D.2b.

Upon combining the positive and negative stiffness mechanisms, an approximate constant torque curve has been generated as presented in Figure D.3

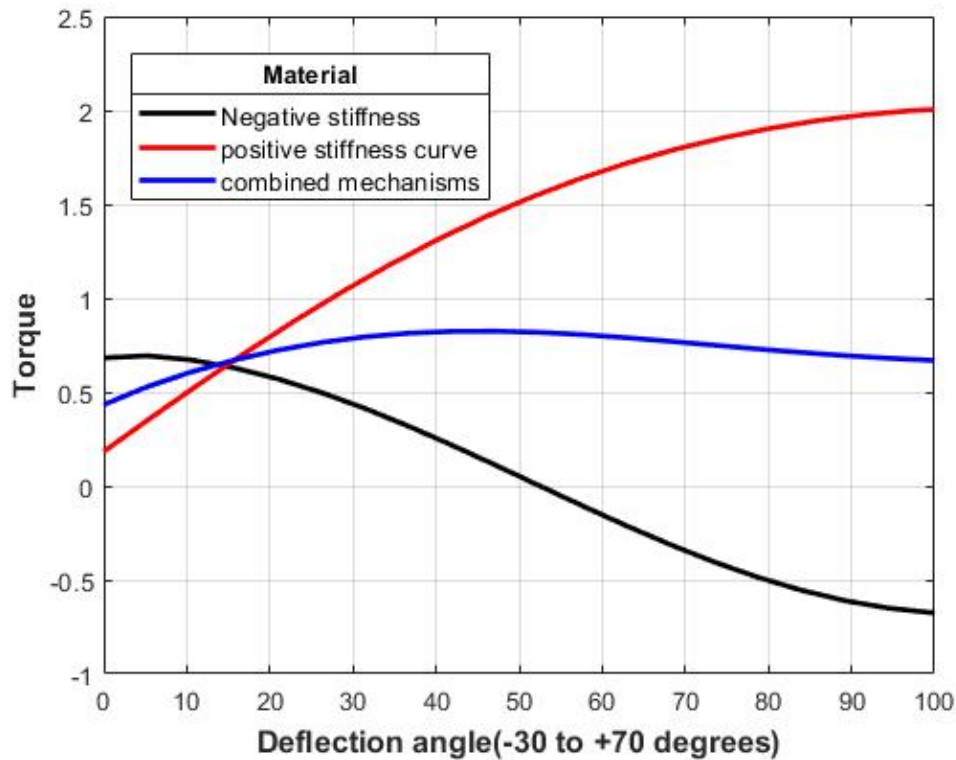


Figure D.3: The torque deflection curve of the combined positive and negative stiffness mechanism.

The analytical results show that the combination of positive and negative stiffness mechanisms has closely approximated a constant torque curve for the compliant mechanism. However, it is important to note that introducing the rubber spring in the negative stiffness mechanism introduces additional moments on the hand. As a nonlinear element, the rubber spring is assumed to be linear.

The linear assumption for the rubber spring may not fully capture its true behaviour, especially at larger deflections. This actual non-linearity of the rubber spring may lead to deviations from the desired results. Moreover, it generates forces that act on the hand as it deflects, and these linear forces can cause additional moments around the hand's centre of gravity, affecting the overall torque output and causing discomfort.

Future studies could incorporate more accurate models for the rubber spring's behaviour to address this limitation, considering its nonlinear characteristics. Experimental testing with real users could also provide valuable insights into the device's performance and comfort during actual use. By refining the rubber spring's model and evaluating its behaviour in more realistic conditions, the compliant mechanism's design can be further optimized to provide better support and enhance the overall user experience.

Moreover, the additional moments caused by the linear forces of the rubber spring should be carefully evaluated in terms of their effect on wrist stability and functionality. By understanding and mitigating these additional moments, the compliant mechanism can be tailored to provide more precise and comfortable support for individuals with muscular disorders, ultimately improving their quality of life and daily activities.